Drought Risk Reduction

Drought Risk Reduction

Z. Su & G.J. Roerink (editors)

Alterra-rapport 1135

Alterra, Wageningen, 2004

ABSTRACT

Su, Z. & G.J. Roerink (editors), 2004. *Drought Risk Reduction*. Wageningen, Alterra, Alterra-rapport 1135. 87 p., 18 figs.; tables.; 37 refs.

Due to the shortage of water resources and its inhomogeneous distribution in space and time, large scale droughts occur frequently all over the world. Consequently, drought has become a key factor constraining the economic development and threatening the food security. This report describes the results of the Drought Risk Reduction project, which aimed at creating an integrated system for the monitoring and evaluation of drought at continental scale. A prototype operational system has been developed by combining remote sensing algorithms (SEBS) with a crop growth model (Rotask) in a data assimilation framework (Ensemble Kalman filter). The developed techniques are tested and partly implemented in the current drought forecasting system of China.

Keywords: drought monitoring, remote sensing, energy balance, crop growth simulation, data assimilation, China

ISSN 1566-7197

This report can be ordered by paying € 35,- to bank account number 36 70 54 612 by name of Alterra Wageningen, IBAN number NL 83 RABO 036 70 54 612, Swift number RABO2u nl. Please refer to Alterra-rapport 1135. This amount is including tax (where applicable) and handling costs.

P.O. Box 47; 6700 AA Wageningen; The Netherlands
Phone: + 31 317 474700; fax: +31 317 419000; e-mail: info.alterra@wur.nl

[Alterra-rapport 1135/December/2004]

Contents

Acknowledgements

This report highlights the main results and conclusions of the *Drought Risk Reduction (DRR)* project, which is funded by the *Water for Food and Ecosystems* sub-program of the *Partners for Water* program of the Netherlands Government.

The following people and organisations were partner in the DRR project consortium and have contributed to this report:

Alterra, Wageningen UR (project leader)
- Prof.Dr. Z. (Bob) Su
- Ir. G.J. Roerink

Plant Research International (PRI), Wageningen UR
- Ir. R.E.E. Jongschaap
- Dr. A.L. Smit
- Ir. M. Paganini

Sub-Department of Water Resources, Wageningen University, Wageningen UR
- Prof.Dr. P.A.A. Troch
- Ir. R.T.W.L. Hurkmans

SarVision
- Dr. P.J. van Oevelen

China Meteorological Centre, China Meteorological Administration (CMC/CMA)
- Dr. Yanbo He

Institute d'Economie Rurale (IER), Mali
- Ir. S. Dione

The cover photo is made by Aart Schrevel.

Summary

Due to the shortage of water resources and its inhomogeneous distribution in space and time, large scale droughts occur frequently all over the world. Consequently, drought has become a key factor constraining the economic development and threatening the food security. The objective of this project is to create an integrated system for the monitoring and evaluation of drought at continental scale and to propose alternatives for drought risk reductions.

The spatial distribution of water can be described by remote sensing techniques; satellite images are one of the very few sources to provide instantaneous information over large continental areas. Alterra has successfully developed the Surface Energy Balance System (SEBS) to estimate drought characteristic parameters by means of satellite remote sensing images. When this information is combined with the crop growth model developed by *Plant Research International* (*PRI*) via data assimilation techniques, a truly dynamic system is then created for the quantification of space-time distribution of water to formulate and implement solutions for water scarcity and food security related problems. The Department of Water Resources of the University of Wageningen provides the data assimilation techniques. SarVision provides the relative soil moisture data derived from active microwave remote sensing. The China Meteorological Centre participated in the prototyping and implementing of the developed system.

The SEBS model has been implemented for the processing of NOAA/AVHRR and MODIS data and evaluation of the codes and the results against field observation data have been carried out. A time series of evaporation fraction images for a whole year is generated with the help of the HANTS algorithm using the results derived from the NOAA data. A time series of relative soil moisture is also generated similarly with the windscatterometer data. These results show that this part of the system is at a prototype stage and can be integrated in an operational environment.

Two retrieval algorithms for relative soil moisture using windscatterometer data are named the Wagner model and the Woodhouse model. Advantages and disadvantages of both methods are discussed. The retrieval algorithms of the two approaches are however considerably different. From the analyses it was difficult to compare both approaches. Although the Woodhouse model is a physically based scattering approach retrieval, the initialization was found to be cumbersome and produced a widely varying result, the Wagner model was preferred in this project because of its extensive testing and clear functionality. Given the range of validity of the Wagner model it is recommended that physically based models like that of Woodhouse et al be investigated further since they can cope with various surface characteristics that the Wagner model cannot in its current form. Validations of both algorithms using field observation data are needed before firm conclusion can be drawn.

The combination of remotely sensed environmental variables with a crop growth model (Rotask 1.5) in a data assimilation framework has been shown with the potential to improve prediction of drought events and consequences for crop yields. Two types of (indirect) observations were selected to be combined with the model simulation: firstly relative evapotranspiration was derived from NOAA/AVHRR data using the SEBS-model, secondly, from passive microwave remote sensing soil moisture content. To integrate observations and model simulation a data assimilation algorithm was selected using the sophisticated Ensemble Kalman Filter (EnKF)

The work that was executed in the Sudano Sahel part of the Drought Risk Reduction project included simulation experiments for adaptation strategies to forecasted droughts or wet climate conditions. A valuable method for Agricultural Strategy Assessment and Early Warning Systems was achieved, by using crop growth simulation models (CP-BKF3), to quantify the effects of adaptation strategies in terms of agricultural production and resource use efficiency. It is shown that, if farmers can be early warned about the type of season they may expect, farmers' anticipation and management strategies can soften the impact of severe climate conditions. It is shown that farmers with a varying access to possible resources are able to anticipate adequately, and reduce their risk on crop failure, but in different ways and in varying degree.

Overall, the project has generated a system that is shown potentially to be able to be used in monitoring, prediction and risk analysis of drought events. More specially the project has achieved the following aims: Increased capacity of scientist in China by means of technology transfer; Generation of a methodology to monitor drought and crop production risks.

1 Introduction

Due to the shortage of water resources and its inhomogeneous distribution in space and time, large scale droughts occur frequently all over the world. Consequently, drought has become a key factor constraining the economic development and threatening the food security. The objective of this project is to create an integrated system for the monitoring and evaluation of drought at continental scale and to propose alternatives for drought risk reductions

The spatial distribution of water can be described by remote sensing techniques; satellite images are one of the very few sources to provide instantaneous information over large continental areas. Alterra has successfully developed the Surface Energy Balance System (SEBS) to estimate drought characteristic parameters by means of satellite remote sensing images. When this information is combined with the crop growth model developed by *Plant Research International* (*PRI*) via data assimilation techniques, a truly dynamic system is then created for the quantification of space-time distribution of water to formulate and implement solutions for water scarcity and food security related problems. The Department of Water Resources of the University of Wageningen provides the data assimilation techniques. SarVision provides the relative soil moisture data derived from active microwave remote sensing. The China Meteorological Centre participated in the prototyping and implementing of the developed system.

The project has achieved to generate a prototype operational system to address the efficient use of water for sustainable food production and food security. Its operation can be realised without too much demand on specific knowledge that is only accessible to professionals. Particular attention is taken care by involving in the project besides research and education organizations also a Dutch commercial firm (SarVision) that is committed to providing operational remote sensing services. Part of the system has been implemented at the China Meteorological Centre in China in combination with its operational system.

Chapter 2 describes the implementation SEBS for the processing of NOAA/AVHRR and MODIS data and evaluation of the codes and the results against field observation data. A time series of evaporation fraction images for a whole year is generated with the help of the HANTS algorithm using the results derived from the NOAA data. A time series of relative soil moisture is also generated similarly with the windscatterometer data.

Chapter 3 describes two retrieval algorithms for relative soil moisture using windscatterometer data. These two methods are named the Wagner model and the Woodhouse model. Advantages and disadvantages of both methods are discussed.

Chapter 4 describes how remotely sensed environmental variables can be combined with a crop growth model (Rotask 1.5) to improve prediction of drought events and

consequences for crop yields. Two types of (indirect) observations were selected to be combined with the model simulation: firstly relative evapotranspiration was derived from NOAA/AVHRR data using the SEBS-model as described in Chapter 2. Secondly, from passive microwave remote sensing soil moisture content as described in Chapter 3. To integrate observations and model simulation a data assimilation algorithm was selected using the sophisticated Ensemble Kalman Filter (EnKF)

Chapter 5 describes the methodolgy developed in the Sudano Sahel part of the Drought Risk Reduction project which seems valuable for Early Warning Systems in the Sahel region, as specific information from farmers' perspective and from environmental settings is taken into account. The simulation model CP-BKF3 in combination with remote sensing observations, enables to upscale results from plot level to districts and regions, which makes forecasts under various scenarios most interesting. Based on remote sensing and/or information stored in geographic information systems, the simulation model may be provided with more detailed information of ground truth (e.g. acreage of millet, sorghum and maize; start of growing season; field locations) in order to enhance early warning systems. The economic consequences of farmers' strategies can be quantified, if outcomes in grain yield are subjected to (local) prices on markets, and the availability and prices of fertiliser. More restraints can be obtained by blocking access to fertiliser markets, or by investigating the closure of irrigation schemes.

Chapter 6 presents the major results of this project and an outlook for the future.

2 Generation of time series of evaporative fractions and relative soil moisture

(Dr. Y. He, Prof.Dr. Z. Su)

2.1 Huabei plane

In China, shortages of fresh water and food resources in 21st century may become very serious. The Huabei plane, located in the Northern part of China is one of the most important grain crop producing areas. These regions belong to semi-arid climate region. Water resources is the key factor for agricultural development and the need for quantitative information on the water balance will increase the areas. Therefore the Huabei plane is choosen as study object.

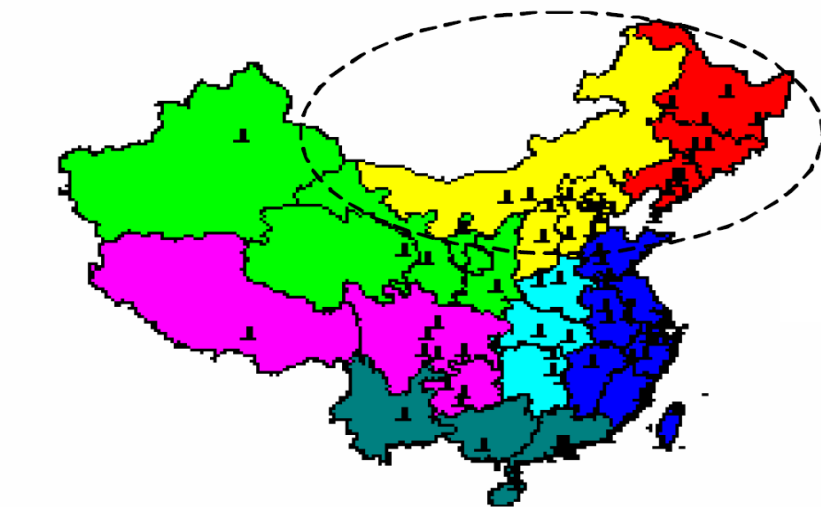

Figure 1 Location of Huabei plane in China

2.2 SEBS

The spatial distribution of water can be monitored with the help of remote sensing techniques. Satellite images are one of the very few sources to provide instantaneous information over large continental areas. Alterra has developed the Surface Energy Balance System (SEBS). This tool calculates maps of the surface energy balance parameters from the satellite images, which indicates how much water stress crops are experiencing at a particular instant in time.

2.2.1 NOAA/AVHRR evaporative fraction calculation

Before SEBS-NOAA (China_Drought version, Su et al, 2003) has been run on NOAA/AVHRR data in 2000, the model code has been checked carefully according to the theoretical formula of SEBS (Su, 2002) and several errors have been corrected. The code modifications are listed in the followings with the codes sections.

After the model code checking for the SEBS-NOAA China_Drought version, the model has been run with the NOAA/AVHRR image data as well as ground meteorological observations.

METEOLOGICAL DATA
The daily meteorological data in year of 2000 have been collected and its elements include Station number, Station longitude, Station Latitude, Station altitude, Surface visibility, Wind speed, wind direction, ambient air temperature, wet-bulb temperature and surface temperature.

NOAA/AVHRR
Totally 192 NOAA/AVHRR images have been collected (Done by Jin Xiaomei) with the total size of 2.19 GB. The data distribution among months in 2000 is listed in Table 1.

Table 1 Data distribution among months in 2000

Month	**Jan**	**Feb**	**Mar**	**Apr**	**May**	**Jun**	**Jul**	**Aug**	**Sep**	**Oct**	**Nov**	**Dec**
File	19	17	13	13	16	15	15	17	19	16	17	15
Size	228	206	156	162	194	180	176	196	218	158	195	172

The details in time distribution of the NOAA/AVHRR data can be find in the Appendix 1.

Among 192 NOAA/AVHRR images, 53 NOAA/AVHRR image data have been processed and their corresponding evaporation fractions also have been calculated by SEBS. Some of the calculation results are listed in Figure 2-2.

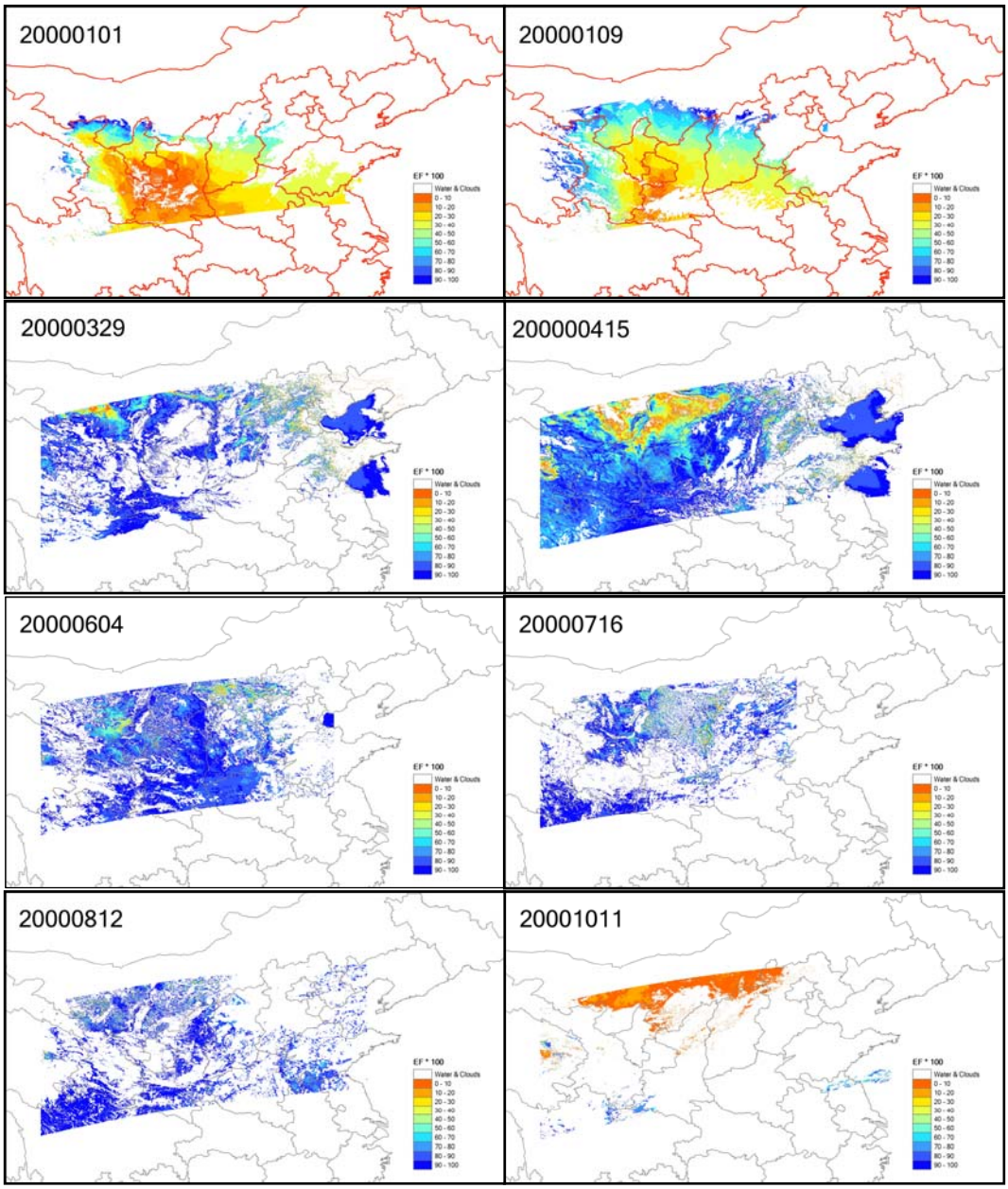

Figure 2-2 Evaporation Fractions calculated from SEBS

2.2.2 HANTS time series analysis

After having the 53 days' evaporative fraction results, a time series analysis has been performed to generate the whole year's time series evaporation fraction. The Harmonic Analysis of Numerical Time Series (HANTS) algorithm is used to perform the time series analysis. It is based on Fourier components, which reflect the start, length and magnitude of the time series behaviour during the year. This algorithm considers only the most significant frequencies expected to be present in the time profiles, and applies a least squares curve fitting procedure based on harmonic components (sines and cosines). For each frequency the amplitude and phase of the cosine function is determined during an iterative procedure. Input data points, which have a large positive or negative deviation from the current curve (like cloudy and missing pixels), are removed by assigning a weight of zero to them. After recalculation of the coefficients on the basis of the remaining points, the procedure is repeated until the maximum error is acceptable or the number of remaining points has become too small. For a detailed description of the HANTS algorithm one is referred to Verhoef (1996) and Roerink et al. (1999).

The parameters value set for HANTS' running is listed below:

- Number Of Frequencies = 4; the selected frequencies were the zero frequency (average) and the frequencies with time periods of 1 year and six months and three months. So the output comprises 7 Fourier coefficients (4 amplitudes and 7 phases).
- Suppression Flag = Low; this flag indicates that low values (outliers) should be rejected during curve fitting.
- Invalid Data Rejection Threshold = +100; this means that evaporative fraction values higher than 100 are rejected (the evaporation fraction has been multiplied 100).
- Fit Error Tolerance = 80 evaporative fraction units; the absolute error in negative direction of the remaining observations should be smaller than 80 evaporative fraction units with respect to the currently fitted curve.
- Degree of OverDeterminedness = 12; together with the minimum of 9 observations this gives that each fitted curve is based on a minimum of 21 observations in time, which is almost half of all data points.

Some of the HANTS derived images are listed in Figure 2-3.

After having the time series evaporation fractions by using HANTS, a movie MPEG file has been generated by using ENVI. The Evaporation faction variability in time and space fits the climate characteristics in Northern China Plain from the first impression of the motivation show.

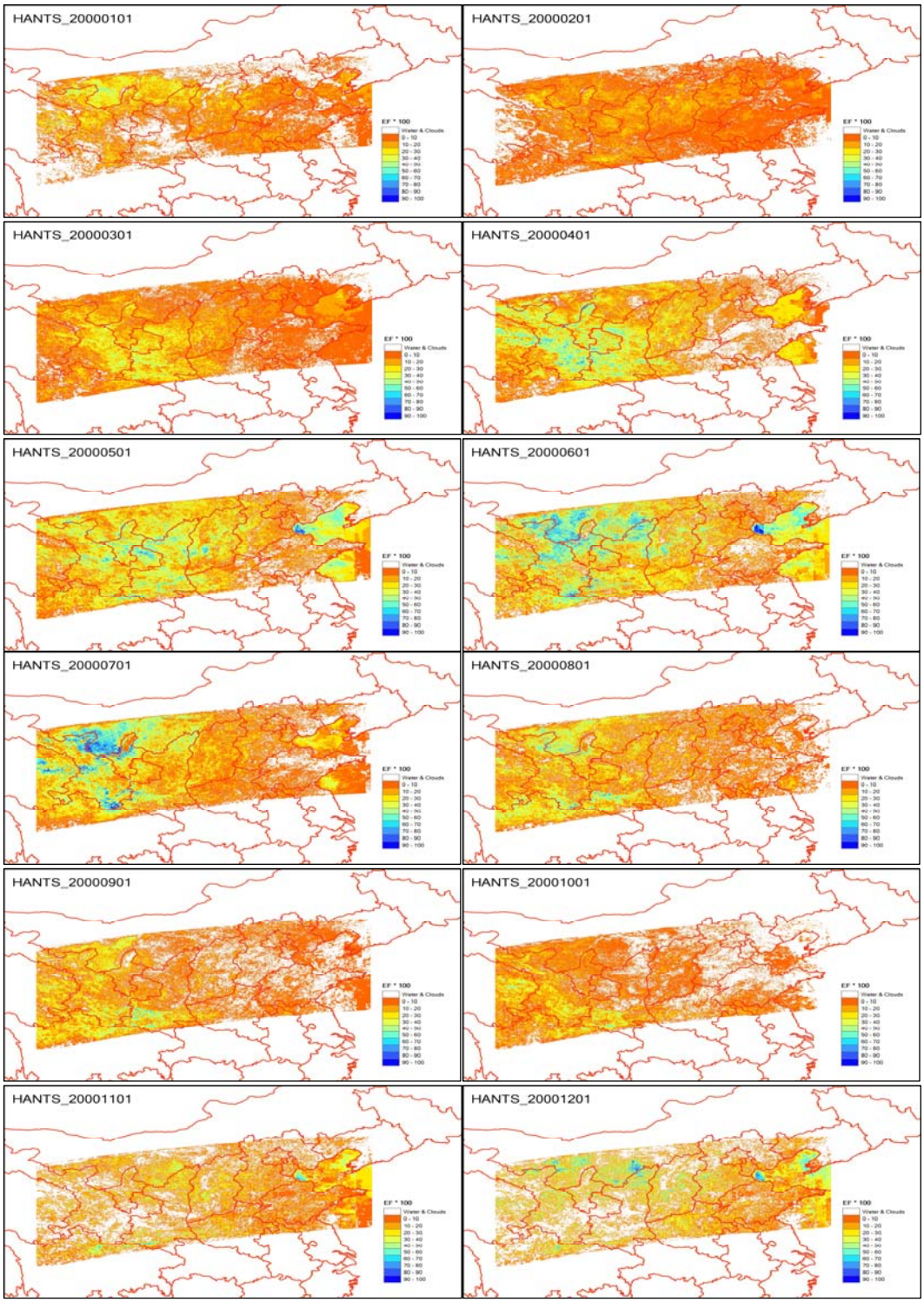

Figure 2-3 The HANTS evaporation fraction simulation results for the first day in each month

2.2.3 MODIS evaporative fraction calcultion

The MODIS instrument provides high radiometric sensitivity (12 bit) in 36 spectral bands ranging in wavelength from 0.4 μm to 14.4 μm, covering the wavelength range of NOAA/AVHRR with finer division in spectrum. The overpass time is around 11:00 AM local time.

The purpose for developing SEBS-MODIS is to use the MODIS data and its products as the inputs for SEBS. The MODIS 1B data (HDF-EOS format) is different from the NOAA/AVHRR 1B data (KLM 1B format) and The SEBS-NOAA can not use the MODIS data directly as its input.

Some results from SEBS can be replaced by the corresponding MODIS products published by DAAC (http://daac.gsfc.nasa.gov/), so the SEBS-NOAA has to been cut down and reconstructed to take the MODIS data products as inputs. The MODIS data products used by SEBS are MOD[03], MOD[09] and MOD[11A1], which provide the information of geo-location, reflectance, temperature and so on.

The following data have been collected and used for the SEBS-MODIS calculations.

MODIS data
The MODIS data products can be downloaded fro the EOS DATA GATEWAY (http://redhook.gsfc.nasa.gov/~imswww/pub/imswelcome/). Till now, 9 days' MODIS data products (0401, 0402, 0403, 0406, 0411, 0412, 0417, 0421 and 0519) have been downloaded from the EOS DATA GATEWAY. The downloaded MODIS data products includes MOD03, MOD09 and MOD11A1, which can provide information of longitude, latitude, sunzenith, reflectance band1 and band2) and temperature for taking as the inputs of SEBS-MODIS.

Meteorological observations
The ground meteorological observations have been collected from National Meteorological Center, China. Since the over pass time of the MODIS is about 11:00 AM in Local time, then the meteorological data has been interpolated linearly from the two times' observations at 08:00 and 14:00 in local time.

Field observations
The 2001 measurements were conducted at the wheat field of Shunyi county, Beijing suburbs, China (40°12'N, 116°34'E). The site was relatively wide with about 700m length and 400m width. The range of LAI was 1.1-2.2 from 13 to 21 April.

The instruments of BREB system included one net radiometer, (manufactured by Jinzhou 322 institute, China); two soil heat plates (developed by China Agricultural University); and Bowen Ratio measuring instrument with sensors-position automatic exchange mechanism (developed by IGSNRR CAS). Air humidity was calculated relying on the dry-bulb and wet-bulb temperatures. Due to the Use of sensors-position auto-exchange technique, there is not systematic bias. The sensors of temperature is made of platinum, the precision is 0.03 ℃ and 0.05 ℃ in laboratory

and in field, respectively. The heights of temperature sensors were 0.6m and 1.6m above the ground, respectively. Two soil heat flux plates was buried at about 1 cm below the ground (one was under wheat row and another was under between rows), the net radiometer was mounted at 2m high over the ground. All data were collected by a data-logger (Data taker, DT100, Australia). The sampling frequency was 15 seconds, the interval of exchanging sensors-position and exporting the averages was 5 minutes.

The EC system consisted of a 3-D ultrasonic anemometer (model DA600, KAIJO Co., Japan), CO2/H2O analyzer was Li-7500, LI-COR Co., USA. They were used for quick measuring vertical wind speed, temperature and humidity, respectively. The system was installed near the BREB observation site. The height of sensors is about 2m above the ground. The data were collected by a high frequency data-logger (DASH-8, USA), the sampling frequency was 20Hz per channel. The averages were recorded every 10 minutes.

Surface infrared temperature sensor was installed at about 2m height, and its angle is about 45 degree, the data was continuously observed, like as radiation, type is BS-32T, 7-20 μm, View angle is 11 degree, it is made in Japan, OPTEX Co. Ltd. the data was recorded with DT100, the same data logger of BR system.

The measurements were made at a wheat field in Beijing shunyi county from 30/03/2001 to 24/04/2001, the following are the illustration of date contents.

A. Bowen ratio

date	date (MMDD, month-date)
Time	time (HHMM, hour-minute)
Th	dry bulb temperature in 1.6m high(C)
Tl	dry bulb temperature in 0.6m high(C)
Eh	vapor pressure in 1.6m high(mb or Hpa)
El	vapor pressure in 0.6m high(mb or Hpa)
Q	Global Radiation(w/m2)
Rk	reflected Radiation (w/m2)
Rn	net Radiation (w/m2)
G1	soil heat flux between wheat line (w/m2)
G2	soil heat flux under wheat (w/m2)
Rn-G	Rn-(G1+G2)/2, (w/m2)
H	sensible heat flux, (w/m2)
LE	latent heat flux, (w/m2)
Br	Bowen Ratio (unitless)
Ts	surface temperature of wheat field (C)

B. Eddy correlation

The sonic instrument was installed at 2m high , Type: DA600, KAIJO Co., Japan; CO2/H2O analyzer: Li-7500, LI-COR, USA, sampling frequency: 20 Hz/channel.

Date	date (MMDD, month-date)
Time	time (HHMM , hour-minute)
Tm	10min mean temperature (C)
Qm	10 min mean absolute humidity (g/m3)
Um	10 min mean wind speed (m/s)
Co2m	(mg/m3)
H_ed	sensible heat flux(w/m2)
LE_ed	latent heat flux(w/m2)
F_co2	CO2 flux(mg/s.m2)
Co2ppm	10 min mean co2 concentration (ppm)
U*	friction wind speed (m/s)

Measuring time is the beginning time, because of the accumulative time errors of eddy data, the eddy-data time may be 0-5 minutes error.

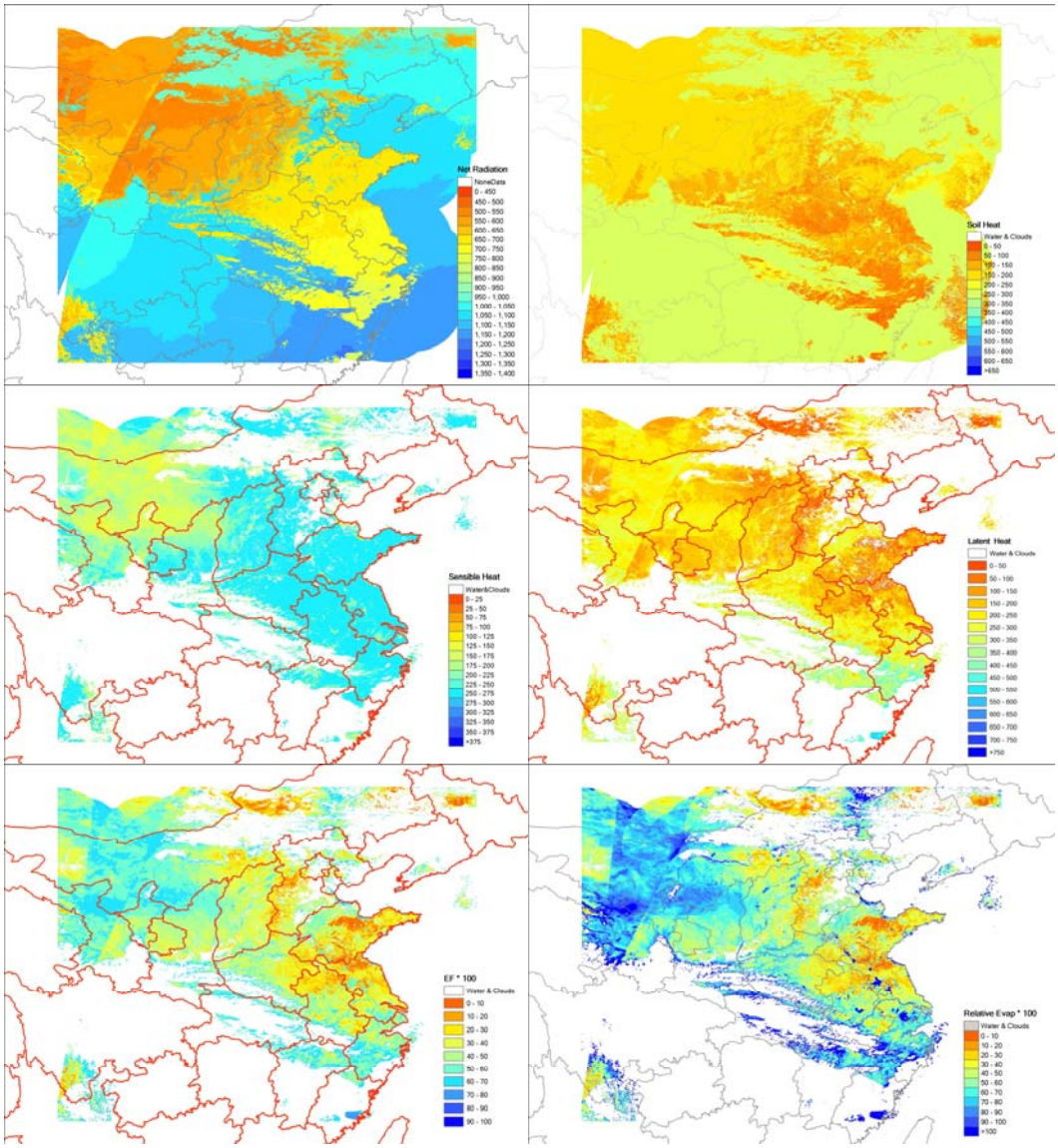

Figure 2-4 Evaporation Fraction calculations on MODIS data of Day 91, 2001

Results

The 9-days MODIS data products have been processed and inputted into SEBS-MODIS. As an example, the results for the Evaporation Fraction calculation on MODIS data of day 91, 2001, are presented in Figure 2-4.

While comparing to the field observations, only 4 days' calculation results are available for comparing. The other days are missing/unavailable of the temperature data and hence have no available calculation results for comparing. Although only 4-days calculation results are not extensive for drawing firm conclusions, the comparing results (Figure 2-5, Figure 2-6, Figure 2-6, Figure 2-7 and Figure 2-8) show that the net radiation has been overestimated as well as the latent heat fluxes. The soil heat fluxes and the sensible heat fluxes calculation results seem much better.

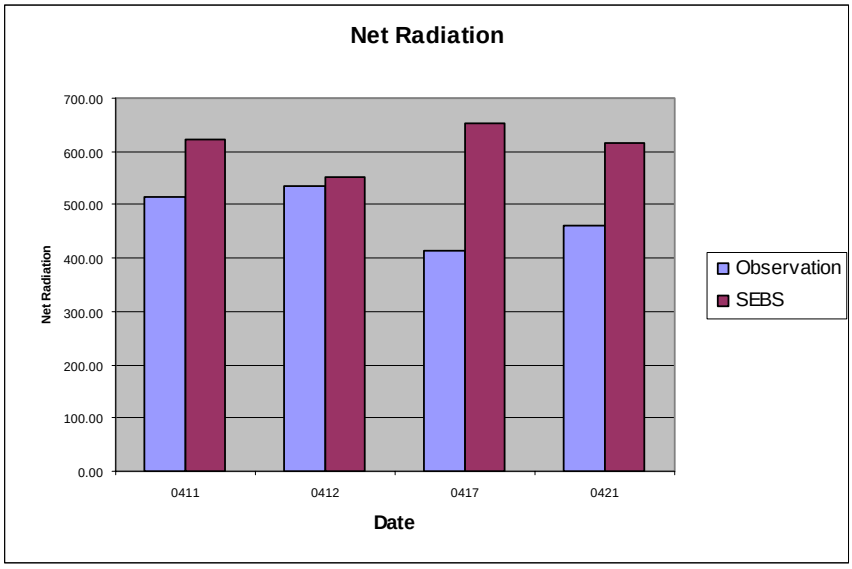

Figure 2-5 Net Radiation (observation vs calculation).

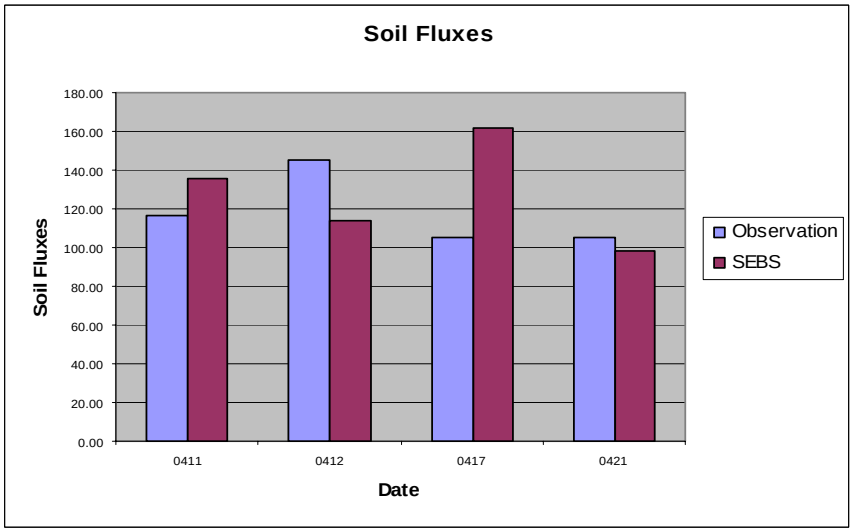

Figure 2-6 Soil Fluxes (Observation vs Calculations).

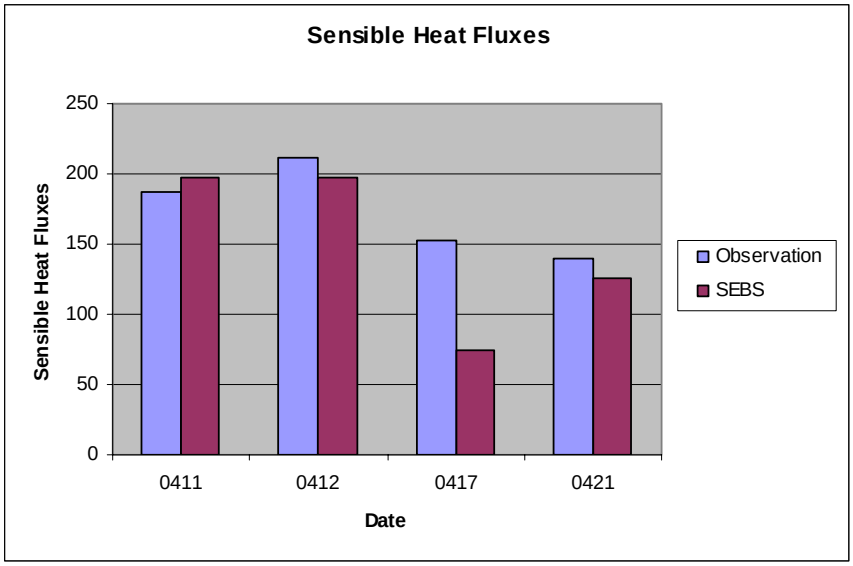

Figure 2-7 Sensible Heat Fluxes (observation vs calculation).

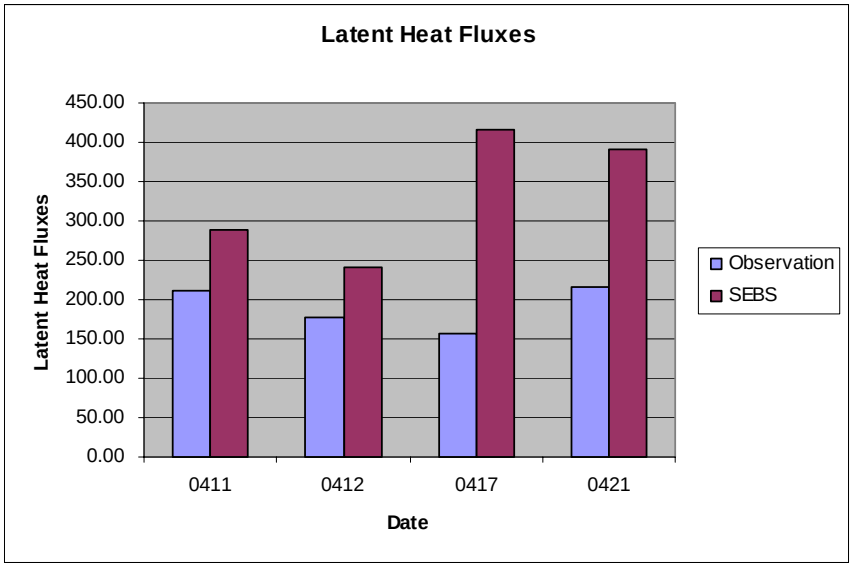

Figure 2-8 Latent Heat Fluxes (Observation vs Calculation).

2.3 Windscatterometer data reconstruction

The Windscatterometer (WSC) data provided by SarVision covers the period 01-01-1992 - 01-01-2001 with the ROI of 100°-125° E and 20°-50° N.

For each decade/month a file (ascii format) is included with the data for the entire ROI, and point coordinates are stored in an extra ascii file (lonlat.txt).

Since the data is stored in the original WSC analysis grid: the grid is defined such that the point spacing is approximately 28 km and the grid definition results in an irregular grid when transformed to geographic coordinates (please note that the resolution of the SWC is still 50 km).

Because of the grid definition is irregular and the ENVI input module can not be used to input the datasets into raster images format.

In order to input the datasets into raster image format, an arc/info AML routine has been developed to map each data points into its original map projection locations according to its corresponding latitude and longitude. Since the projection information for the original grids have not been attached to the datasets and also have not been specified by SarVision, who provided the datasets, an Albers projection with the following parameters has been assumed in this situation:

PROJECTION Albers
UNITS meters
DATUM WGS84
PARAMETERS
25 00 00.0
47 00 00.0
110 00 00.0
0 00 00.0
0
0

After having the projection-restored raster images, all the images further have been converted into geographic projections with the resolution of 0.03 degree.

After having the geographic projection information, all the soil water content (SWC) images for decade/month have been stacked (stacking.pro) into two ENVI image files for decadal and monthly SWC data respectively.

In Appendix 2 the program lists and directory structure of the NOAA/AVHRR, MODIS and WSC results are shown.

3 ERS Windscatterometer data for soil moisture estimation in China

(Dr. P.J. van Oevelen)

3.1 Introduction

This study aims at exploring two techniques currently available to estimate surface soil water content by means of remote sensing. Soil moisture is a key variable that links the energy and water cycle over land surfaces and is in part responsible for the partitioning of available energy into latent and sensible heat. Good knowledge on the status of soil moisture can thus contribute greatly to tackle problems in water (resources) management.

3.2 Methods and Materials

The ERS Windscatterometer is a C-band radar (frequency is 5.6 GHz) with a spatial resolution of approximately 50 km with a high sampling rate on board of the European Remote Sensing (ERS) satellite. The first satellite, ERS-1, was launched in 1991 and was decommissioned in 2000 and was followed up by ERS-2 in 1995 with a similar instrument configuration. With the launch of the METOP platform in the near future a successor of the Windscatterometer will become available.

3.2.1 Model of Wagner et al.

This model is a semi-empirical approach with a strong change detection component to estimate the surface soil moisture content over a resolution cell.

To retrieve surface soil moisture they (Wagner et al., 1999a, b) compared the backscattering coefficient extrapolated to a reference angle at 40° denoted $\sigma°(40)$ to the highest and lowest values of $\sigma°(40)$ ever measured, which for each pixel were extracted from long backscattering series (in their case at least 6 years of data). The lowest backscatter observed $\sigma°_{dry}(40,t)$ was associated with no liquid water present and the highest $\sigma°_{wet}(40,t)$ was presumed to be saturated with liquid water. The wettest backscattering coefficient was found to be more or less constant over time and independent of vegetation cover while the lowest backscattering coefficient showed seasonal trends coinciding with vegetation growth. Assuming a linear relationship between backscattering coefficient and soil moisture the relative moisture content in the surface layer ms is calculated with:

$$m_s = \frac{\sigma^0(40,t) - \sigma^0{}_{dry}(40,t)}{\sigma^0{}_{wet}(40,t) - \sigma^0{}_{dry}(40,t)} \qquad (3\text{-}1)$$

Where m_s is a relative measure of soil moisture content in the surface layer ranging between zero and one or 0 and 100%. Using these results a soil wetness indicator (SWI) was developed based upon an exponential drying function (infiltration model) of the top 1m of soil to have indicator of root zone available water.

This SWI model has been applied globally and seemed to follow the available surface soil moisture trend and surface moisture indicators well within bounds of the applicability of the data.

The validity of applying the model is limited to certain areas. Example given over tropical forests and regions of azimuthal anisotropic surfaces (normally sand deserts) soil moisture retrieval is not possible. The retrieval is furthermore not possible under frozen/snow conditions.

Since the SWI is a relative measure of soil moisture ranging between 0 and 100. The study over the Ukraine (Europe) has shown that 0 corresponds to the wilting level and 100 to a value in-between field capacity and total water capacity (Wagner et al., 1999 a).

The model is well documented and data is freely available with good instructions on the applicability of the data.

3.2.2 Model of Woodhouse et al.

This model is a more physically based inversion approach using a scattering model to estimate the various contributions (vegetation cover, reflectivity and RMS slope) to the scattering from which a surface water content is derived.

Description of the Forward Model

In endeavouring to retrieve geophysical parameters from the WSC data, it is necessary to develop a forward model that account for those effects considered important at C-Band VV and which are relevant for the region under observation. In our treatment, the resolution cell is represented by an equivalent surface consisting of a combination of only two surface types: dense, homogeneous vegetation (pure volume scattering) with a fractional surface area denoted by C, and bare soil with effective (homogeneous) roughness and dielectric properties (surface scattering). The total backscatter is therefore considered to be an incoherent sum of three backscattering mechanisms: these are (vegetation) volume scattering, surface scattering from the bare soil layer, and specular (double-bounce) reflection between the trunk and ground. In addition, a fourth term may be added which accounts for all other contributions not included in the first three. Since this term may include contributions from such features as highly specular surfaces, its overall effect may be to reduce the total observed backscatter, so that it may be considered to be a random error on the forward model calculation.

Specific models are adopted for each component separately, and their contributions are calculated for an incidence angle, θ_i and azimuth angle φ_i and are summed incoherently so that

$$\sigma^o(\theta_i,\varphi_i) = C\sigma^o{}_{cover} + [1-C]\sigma^o{}_{bare} + \sigma^o{}_{double} + \sigma^o{}_{other} \qquad (3\text{-}2)$$

where,

$\sigma^o(\theta_i,\varphi_i)$	=	scattering coefficient measured at the WSC,
C	=	equivalent fractional vegetation cover,
$\sigma^o{}_{cover}$	=	contribution from equivalent vegetation cover (modelled by a direct backscatter term which corresponds to volume scattering),
$\sigma^o{}_{double}$	=	contribution form double-bounce scattering, and
$\sigma^o{}_{bare}$	=	contribution from equivalent bare soil.

The individual contributions may be modeled in a number of different ways, from simple empirical models to elaborate radiative transfer models. In the current study, the nature of the investigation is to monitor an area with limited ground data and with a high degree of variation in surface parameters. A simple approach was therefore adopted in order to illustrate the applicability of this method, and to highlight the potential of using WSC data. The component nature of this model allows for more advanced models to be incorporated at a later date.

With the additional use of general *a priori* constraints an optimal estimation (or maximum likelihood) inversion method may be used to infer estimates of the unknowns (Rodgers, 1976).

For further discussion of this method, see Woodhouse et al., (1999 and 2000), and Van Oevelen and Woodhouse, 1996.

3.3 Results and Analysis

Both of the models were applied over the Chinese region. Special attention was given to the model of Woodhouse et al. since numerous problems occurred in applying the data. Firstly due to a changed format in the windscatterometer data received it took considerable time to verify if the data was correctly being read.

In applying the mode it requires to state the initial surface conditions on which the model iterates towards a solution. Since the region is not well known to the authors a first guess was applied and consequently changed to see the effects. Unfortunately, the results were not consistent and difficulties arose in the applicability of the model in its current state.

While the Woodhouse model described here is relatively simple and makes many assumptions about the surface characteristics under observation. It was unclear if the retrieved values of vegetation cover that fall within the expected range. They however did not exhibit temporal and spatial patterns compatible with data from other sources. We contribute this to a wrong initialization of the model. The retrieved parameters of reflectivity, while having magnitudes varying much more than might be expected, do indicate relative temporal and spatial variations that are most likely related to surface soil moisture content. However these were not consistent with those found by Wagner et al. model.

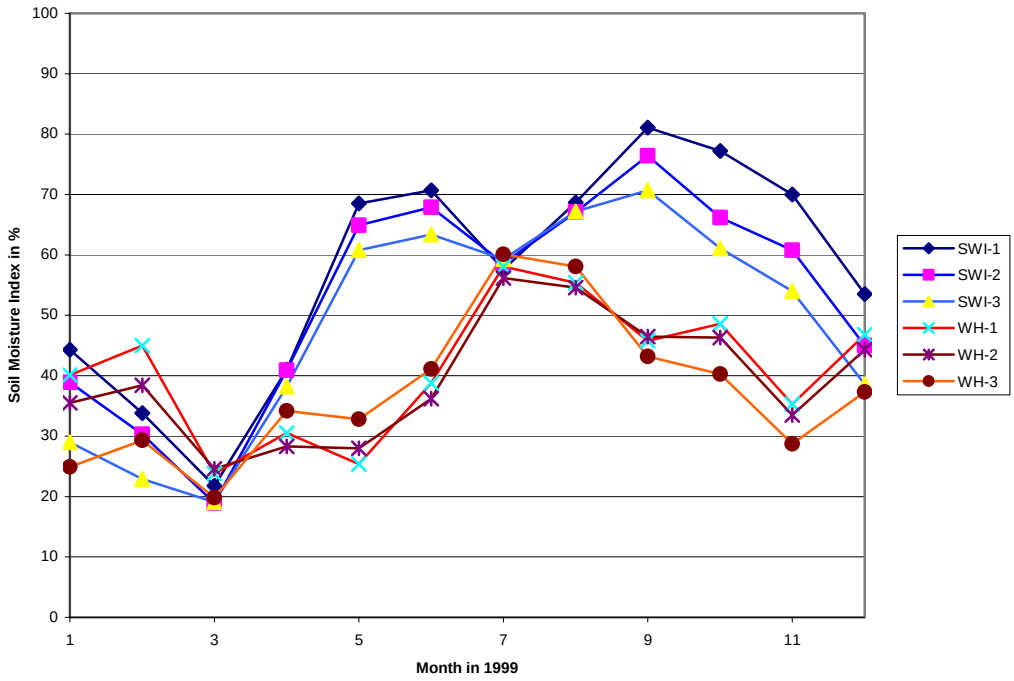

Figure 3-1 Comparison for three locations in China of soil moisture retrieved from Windscatterometer data where the Wagner Soil Moisture Index is indicated by SWI-# and the corresponding values from the Woodhouse model by WH-#.

In Figure 3-1 a comparison for three locations is given for the two models. Clearly it can be seen that the Woodhouse model predicts in general lower values and does not follow the trend from Wagner model nor do the peaks coincide. Furthermore, in particular location #3 (SWI-3 and WG-3) seems to be conflicting.

Full comparison with the Wagner data was deemed inappropriate since both models use different approaches and estimates different values. The Woodhouse model the surface reflectivity which is related to surface soil water content and the Wagner model gives the SWI which represents the water content over 1 m of soil.

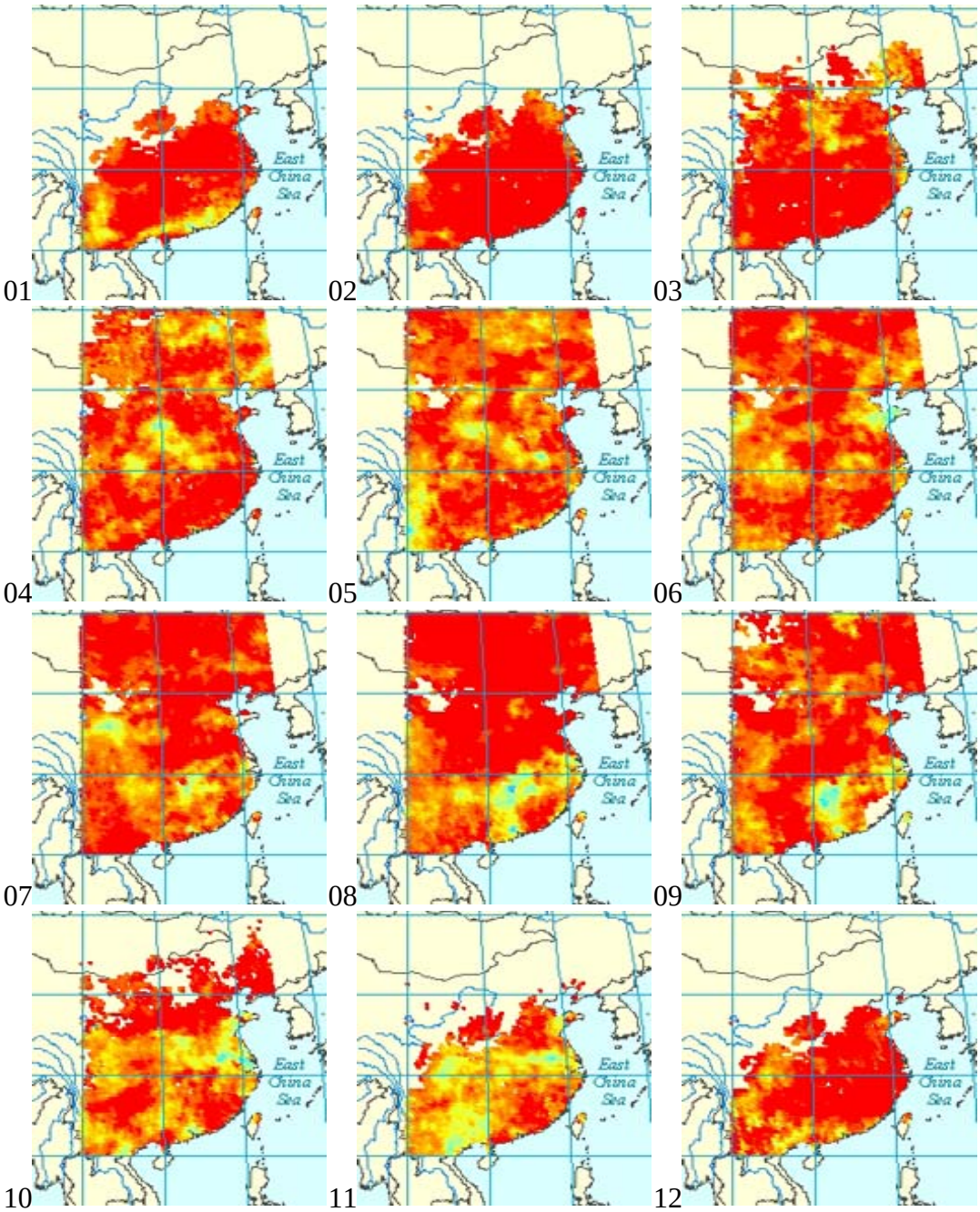

Figure 3-2 Soil Wetness Index variation over China from the Wagner model during the year 1999 where 01 depicts January to 12 being December. The colourless areas indicate no valid data available.

In Figure 3-2 the variation of soil moisture as represented by the Soil Wetness Index is given for monthly means over a large part of China for the year 1999. Clearly consistent changing patterns can be found, however note that during the winter months larger areas of invalid model output can be observed (depicted by no values in Figure 3-2).

The Woodhouse model however is an elegant solution that given the time constraints unfortunately could not be explored to the maximum extent needed. The efforts required to validate the results of the model fall outside the resources available within this project. Hence, given the extensive testing of the Wagner model and its ease of use and applicability it was decided to use and make available this data product to the project.

3.4 Discussion and Recommendations

The retrieval algorithms of the two approaches are considerably different. From the analyses it was difficult to compare both approaches. As stated in the results the data of the Wagner model was preferred here because of its extensive testing and clear functionality. Although the Woodhouse model is a physically based scattering approach retrieval, the initialization was found to be cumbersome and produced a widely varying result.

Given the range of validity of the Wagner model it is recommended that physically based models like that of Woodhouse et al be investigated further since they can cope with various surface characteristics that the Wagner model cannot in its current form. An elegant solution might be the combination of the two approaches where change detection is combined with a physical model.

Acknowledgements
The authors thank Manuela Grippa, Iain Woodhouse and Marc LeBlanc for their support during this study.

4 Implementation of an Ensemble Kalman filter data assimilation algorithm into a crop growth model

(Ir. R.T.W.L. Hurkmans, Prof.Dr. P.A.A. Troch)

4.1 Introduction

Drought is one of the major environmental disasters in various parts of the world, generally characterized by abnormal soil water deficiency. This is mainly caused by natural climatic variability, such as precipitation shortage or increased evapotranspiration. Since these climatic factors have a large spatial and temporal variation, it is hard to monitor or predict drought events. Remote sensing, however, can help to do so due to its large spatial scales and frequent coverage (Su et al., 2003).

In the framework of the Drought Risk Reduction (DRR) project a crop growth model was used to simulate crop growth and investigate consequences of soil water deficiencies for crop growth. In this study, remotely sensed monitoring of related environmental factors is combined with the crop growth model to improve prediction of drought events and consequences for crop yields.

Fifteen pilot fields in northern China were selected, for which the crop growth simulation model Rotask 15 (Jongschaap, 1996) was used to simulate winter wheat growth. Two types of (indirect) observations were selected to be combined with the model simulation: firstly relative evapotranspiration was derived from NOAA/AVHRR backscatter data using the SEBS-model according to Su, 2002 and Su et al., 2003. Secondly, from passive microwave remote sensing soil moisture content can be derived according to Wagner, 1999, resulting in the dataset that was used here containing the Soil Water Index. More information about the datasets can be found in Section 4.2.4.

To integrate observations and model simulation a data assimilation algorithm was selected. A variety of such algorithms have been proposed, ranging from rather simplistic algorithms (Paniconi et al., 2003; Marrocu and Paniconi, 2001;McLaughlin, 1995) to sophisticated algorithms such as the Ensemble Kalman Filter (EnKF) that is used here (Reichle et al., 2002; McLaughlin, 2002; Evensen, 2003; Crow and Wood, 2003). In the EnKF the model is simulated several times in short periods (from observation time to observation time) in which initial and boundary conditions are slightly varied to create an ensemble of simulations. Using statistical characteristics of the simulation ensemble and the observation the model state is updated.

In the next section some more detailed information is provided concerning data assimilation in general and specifically the EnKF, the crop growth model Rotask and the available observed datasets. In Section 4.3 the methodology of the implementation of the EnKF and its application according to the three possibilities

mentioned above is explained, in Section 4.4 the results are described, in Section 4.5 they are discussed and at last some conclusions will be drawn in Section 4.6.

4.2 Theory

4.2.1 Data assimilation

Data assimilation is a technique to provide physically consistent estimates of the state of a given variable. The estimates are time dependent and spatially distributed and derived from scattered observations at different times and locations, supported by additional data such as prior knowledge of the system, e.g. climatology, and error covariance of both the model and the observations. Including this observation data and the model simulated information, the assimilation methodology should be able to improve the predictive skill of the hydrological model. Besides providing a better estimate of the initial condition of the system state, a data assimilation procedure should be able to assimilate measurements during the model simulation every time new data become available. This is called four-dimensional data assimilation (4DDA) (Marrocu and Paniconi, 2001).

A range of data assimilation methods has been developed; some relatively simple examples are direct insertion, where the model variable is simply replaced by the observed value, and statistical correction, where model mean and variance are adjusted to observation mean and variance (Marrocu and Paniconi, 2001). Some more advanced methods are 4DDA methods like Newtonian nudging (Paniconi et al., 2003 and Marrocu and Paniconi, 2001) and the Kalman filter, which is of interest here and explained in more detail below. For an overview of assimilation methods and studies we refer to van Loon and Troch, 2001, and McLaughlin, 1995.

4.2.2 The Ensemble Kalman Filter

The classical Kalman filter assumes the state equation to be linear and the probability density functions to be Gaussian, which makes it possible to compute the propagated mean and covariance of $x(t)$ from the state equation and the means and covariances from the input errors. Since hydrologic problems are often highly non-linear, they can be solved by repeated linearization. In such a case the algorithm is called the extended Kalman filter. Unfortunately, in case of highly non-linear problems the model proves to be very unstable due to the linearization (Miller, 1994). This problem can be solved by using another adaptation, namely the so-called Ensemble Kalman Filter (EnKF). This approach uses a synthetically generated ensemble of random replicates to capture some of the information contained in conditional probability density functions. One version of an ensemble filter is shown in Figure 4-1. At the initial time t_0 an ensemble of random replicates is generated for each uncertain input appearing in the state equation. This initial condition ensemble is used to derive a corresponding ensemble of state vector replicates at the first measuring time t'_1. In Figure 4-1 replicate j of the 'state' ensemble is written as $x^j(t'_1)$. At t'_1 sample statistics such as means and covariances are derived from the members

of the propagated state vector ensemble. They are used to compute an updated state $x^j(t'_1 | Z_1)$ which is conditioned on the first observation Z_1.

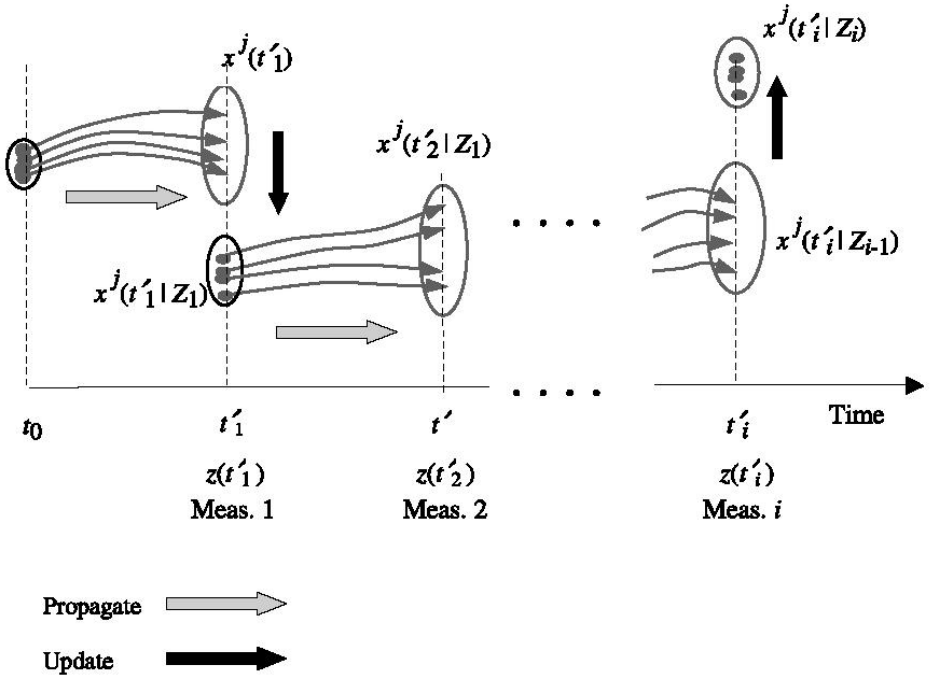

Figure 4-1 Ensemble filtering. Each replicate of the ensemble is propagated forward to the next measurement time and then updated to reflect the influence of the new measurement (McLaughlin, 2002).

Updating occurs according to Equation (4-1):

$$X_+ = X_- + \left(\frac{\sigma^2_{\text{mod}}}{\left(\sigma^2_{\text{mod}} + \sigma^2_{obs}\right)}\right) * \left[X_{obs} - X_-\right] \qquad (4\text{-}1)$$

in which X_+ and X_- are the model state after and before (averaged over the ensembles) the update respectively, X_{obs} is the observed state, σ^2_{mod} is the variance of the model prediction error and σ^2_{obs} is the variance of the observation error. The factor containing the three variances determines the weight of the observations with respect to the model simulations and is also called the Kalman gain. After updating the propagation-update sequence is repeated for each measurement time (Schuurmans et al., 2003; Reichle et al., 2002).

Although the ensemble Kalman filter does not require the equations to be linear, its assumption that the propagated density is Gaussian is likely to be correct only when linearity applies and all errors are normally distributed with a mean of zero. When the problem is nonlinear the EnKF will thus usually be sub-optimal, although estimates may still be reasonable because the sample covariances partly reflect the effects of non-linearities in the state and measurement equations. In any case the flexibility of the method makes it an attractive option for data assimilation applications. Since this approach does not require the state equation to be linear and the model input errors

generated during the propagation step to be additive, it makes the EnKF much more flexible than any of the alternatives.

4.2.3 Crop growth model: Rotask 1.5

Rotask 1.5 was used to simulate winter wheat growth at 15 fields in northern China, the relative locations and coordinates are shown in. For each field several types of input data were required by the model, such as soil data concerning hydrology and chemistry, meteorological data and management data (irrigation, ploughing, fertilizing etc). For application to the fields, the soil profile was divided in seven layers (Table 2). For each of the layers the soil data contained hydraulic conductivity, soil water content at wilting point, field capacity and saturation and carbohydrate and nitrogen contents. The meteorological data was collected from one meteorological station in the area where the fields were located and contained minimum and maximum temperature, incoming short-wave radiation, precipitation, water vapor pressure and wind speed. In Appendix 4 some of the meteorological variables (precipitation, temperature and incoming radiation) are shown. For detailed information about the functioning of Rotask 1.5 and what further in-and outputs it requires, see Jongschaap, 1996.

Table 2 Division of the 2 m soil profile into 7 layers with their depths.

Layer nr.	1	2	3	4	5	6	7
Thick [cm]	2	3	5	10	20	40	120

As output the model provided, among others, actual and potential evaporation and actual and potential transpiration. With these variables Relative Evapotranspiration (RET) can be computed by means of Equation (4-2):

$$RET = \frac{(act.\,evapotranspiration)}{(pot.\,evapotranspiration)} \qquad (4\text{-}2)$$

Since application of the model with the EnKF required the model to simulate time intervals between observations instead of a whole growing season at a time, it was necessary to change the model. At the end of each interval all crop state variables that indicate development stage and time of the crop growth have to be saved and used to reinitialize the next simulation, otherwise the model would use the value that the state variables had the first day for every day of the simulation. The same holds for the soil moisture content in each of the layers.

In Figure 4-2, the RET is shown for three different model simulations, for the whole growing season, using intervals of 1 day and 10 days respectively, and one simulation where the whole growing season is simulated in one time (with the original model). Ideally all simulations should be identical, but as it appears they are not. Especially at the end of the period, where the influence of vegetation becomes significant, the simulations deviate strongly. The crop routine in the model is still not properly

reinitializing the vegetation state variables at the start of each interval. Because of this effect and also due to the fact that observations (see Section4.2.4) were only available for the year 2000 (until day 366 in Figure 4-2), we chose to use only the year 2000 for the analysis.

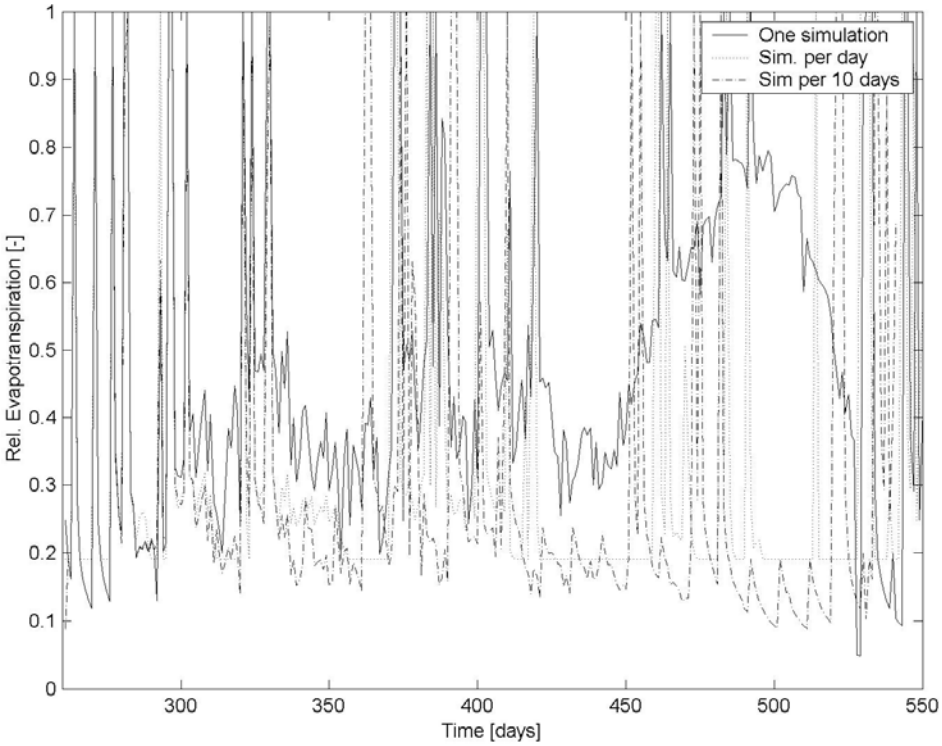

Figure 4-2 Three different simulation of the experiment period (the days count from January 1st 2000). The solid line represents the original model (whole growing season at once), the dashed line is the simulation in stretches of 10 day, and the dotted line is the simulation from day to day.

Although also in this part the simulations deviate, it is not as strong as in the latter part of the period. The 10 day intervals seen to stay closer to the original simulation and also show more of the model dynamics (the day-to-day simulation showed a threshold at about 0.2, where it was constant for rather large sections of the simulation. Besides, one of the observation datasets (SWI) was only available as 10-day averages. Therefore we chose to simulate the model using 10 day intervals.

4.2.4 Observation datasets

Two datasets were selected to be used as observed datasets, although none of them consisted of direct observations but were produced by other algorithms from remote sensing observations as is explained in the following sections.

Relative Evapotranspiration (RET)

The first dataset that was used was Relative Evapotranspiration (RET) data. This dataset was computed by the Surface Energy Balance System (SEBS) from remote sensing data in the visible, near infrared and thermal infrared frequency range, a dataset of several meteo-data at reference height and the downward long wave and short wave radiation. (Rauwerda et al., 2002). For more information about SEBS and the procedure to derive relative evapotranspiration, see Su, 2002, Li et al., 2003 and Su et al., 2003. However, in the period corresponding to the simulation period of the Rotask-model only 6 days of RET data was available, and due to cloud contamination available data was very sparse over the area. Pixels containing usable data didn't correspond to the locations of the fields for which the model simulation took place.

Therefore the available data was interpolated (a smooth curve is fitted through the available data points) using the Harmonic Analysis of Time Series (HANTS) algorithm, providing workable data for the Ensemble Kalman filter. After interpolation, RET data is available on a daily base for every pixel in the area. For more information about the HANTS and its applications, see Roerink and Menenti, 2000. There are disadvantages of the approach of interpolating with HANTS: it is questionable of the interpolated data is representative when so few data are available and the peaks in RET that correspond to rainfall events that occur in the model simulations are smoothed out in the interpolated product.

Soil Water Index (SWI)

As a second observed value the Soil Water Index (SWI) was used. This is a relative measure of soil moisture ranging from 0 to 100 and is derived from the ERS scatterometer. For more information about the derivation of the SWI, see Wagner, 1999. The analysis to derive SWI is however point-based; resulting in point values representing a satellite footprint. Research has shown that a SWI value of 0 corresponds to the soil moisture content at wilting point and a value of 100 to the soil moisture content at a value in between field capacity and total water capacity. It is a measure of the soil moisture content in the upper one meter profile of the soil. SWI observations are available as averages over a 10-day period.

4.3 Methodology

To give an idea of the spatial distribution of the 15 fields at which the analysis took place and the locations of the SWI observation points, they are shown in. RET observations were available over the whole area that is shown in.

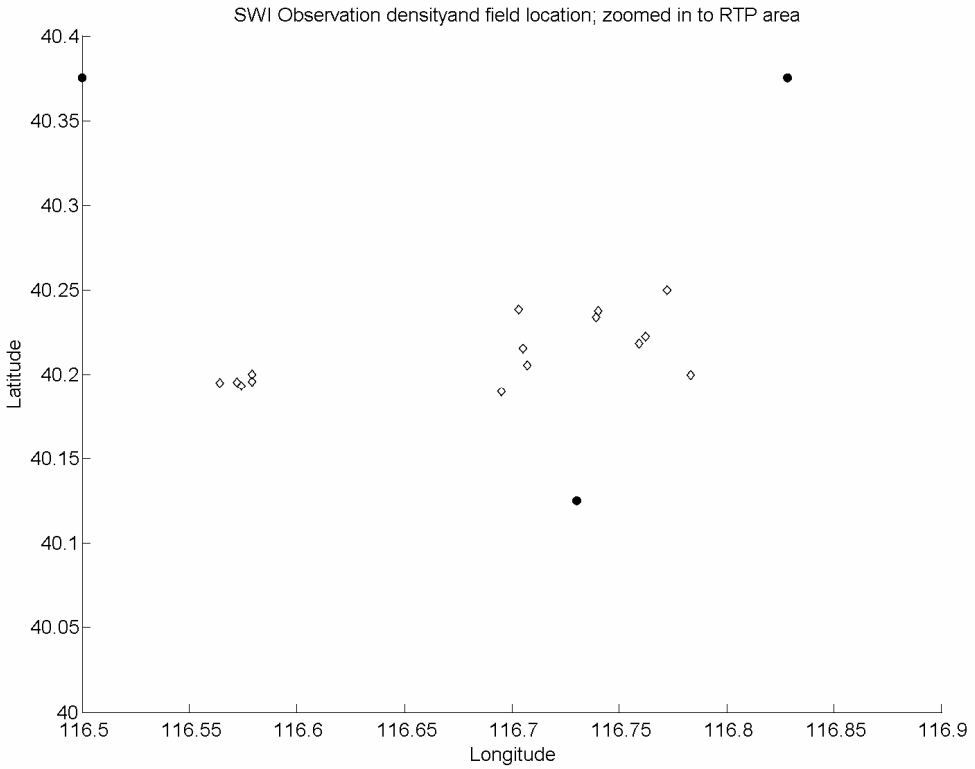

Figure 4-3 The area (0,4 x 0.4 degrees) defined about the 15 fields. The open dots represent the fields; the solid dots are SWI observation points. In the whole area relative evapotranspiration data was available.

RET observations were available on a daily base, but for reasons explained in Section 4.2.3, the model was run using 10-day intervals, so only one RET observation per 10 days was used. A guess-value (0.18) was used for initial soil moisture and by subtracting or adding a percentage of this initial value (see Table 3) an ensemble of 5 members was created. In addition, for each simulation 5 different values for precipitation and 5 values for temperature were created according to Table 3, leading to an ensemble of 125 members. The variation of temperature and precipitation over the ensembles is shown in Figure A.4 in Appendix 4. The model and EnKF were applied with each of the two available datasets: RET and SWI.

Table 3 Creation of the ensemble for the EnKF: precipitation values, temperature and initial soil moisture content were varied.

Precipitation Range [mm\day]	**Calculation from original for each ensemble member**				
	1	**2**	**3**	**4**	**5**
Precipitation	-20 %	-10 %	-	+10 %	+ 20 %
Temperature [°C]	**Calculation from original for each ensemble member**				
Min. Temp.	-20 %	-10 %	-	+10 %	+ 20 %
Max. Temp.	-20 %	-10 %	-	+10 %	+ 20 %
Init. soil moist. Content [-]	**Calculation from original for each ensemble member**				
	-10 %	-5 %	-	+5 %	+ 10 %

4.3.1 Using the EnKF with RET observations

In this case the updated state variable was RET. After every 10-day interval for each ensemble member RET was computed using Equation (4-2). The ensemble average was then updated with the RET observation following Equation (4-3):

$$RET_{UPD} = RET_{SIM} + \frac{COV_{SIM}}{COV_{SIM} + COV_{OBS}} * (RET_{OBS} - RET_{SIM}) \qquad (4\text{-}3)$$

where RETUPD, RETSIM and RETOBS are respectively the updated relative evapotranspiration, relative evapotranspiration as simulated by the model, and the observed relative evapotranspiration. COVSIM was the variance of the prediction error of the model simulation and COVOBS was the variance in the observation error. As the observed value RETP at one pixel, the one that corresponded to the field coordinates was used.

It was impossible to quantify COVSIM and COVOBS thoroughly since no data was available of model simulation and observations: there was no ground truth and the observations had undergone extensive processing. Therefore, according to Schuurmans et al., 2003, a ratio between the two error covariances was established:

$$B = \frac{COV_{SIM}}{COV_{OBS}} \qquad (4\text{-}4)$$

When Equation (4-4) is substituted in Equation (4-3), this yields:

$$RET_{UPD} = RET_{SIM} + (\frac{B}{B+1}) * (RET_{OBS} - RET_{SIM}) \qquad (4\text{-}5)$$

Because there was no ground truth or other kind of measurement, there was no criterion to evaluate the value of B with: if the observations would be used as a criterion the largest value of B would be the best. Therefore we assumed that the uncertainties in model and observation (which are no direct observations) are of the same magnitude, i.e. B = 1.

Since RET is no direct input to Rotask 1.5, the updated RET needed to be converted to soil moisture content to reinitialize the model. According to Su et al., 2003, relative soil moisture can be assumed equal to relative evapotranspiration since the portion of water that evaporates (actual over potential) is limited by the amount of water in the soil, i.e. the relative soil moisture content. Since for each field soil data contains soil moisture content at wilting point and field capacity, actual soil moisture content could be derived from relative soil moisture content according to:

$$VSM = (VSM_{REL} * (VSM_{FC} - VSM_{WP})) + VSM_{WP} \quad (4\text{-}6)$$

where VSM is the actual volumetric soil moisture content, VSMREL the relative soil moisture content (thus equal to relative evapotranspiration) and VSMFC and VSMWP are soil moisture contents at field capacity and wilting point respectively. From the resulting VSM a new ensemble was created in a similar way as the initial ensemble and the model is reinitialized for the next simulation interval.

4.3.2 Using the EnKF with SWI observations

From the model output again the relative evapotranspiration was computed and subsequently converted to VSM according to Equation (4-6), for each ensemble member.
Then, the averaged VSM is updated using the VSM derived from the observations using Equation (4-7):

$$VSM_{UPD} = VSM_{SIM} + (\frac{B}{B+1}) * (VSM_{OBS} - VSM_{SIM}) \quad (4\text{-}7)$$

where, VSMUPD, VSMSIM and VSMOBS are respectively the updated, simulated and observed VSM. B is the fraction between error covariances of model and observation (Equation (4-8)). To obtain VSMOBS, SWI was converted to VSM. Since it is an index ranging from 0 to 100 where 0 is soil moisture at wilting point and 100 is in between field capacity and saturation (Wagner, 1999), SWI can be converted to VSM according to Equation (4-8):

$$VSM = VSM_{WP} + \frac{SWI}{100} * ((VSM_{FC} + \frac{VSM_{SAT} - VSM_{FC}}{2}) - VSM_{WP}) \quad (4\text{-}8)$$

where VSMWP, VSMFC and VSMSAT are soil moisture contents at respectively wilting point, field capacity and saturation. Since SWI was only representing the upper meter of the soil profile, only the upper 6 layers of the modeled soil profile were used, corresponding to 80 cm. The updated VSM was averaged over the 6 soil layers and a new ensemble for the next interval was composed according to Table 3.

4.4 Results

In this Section the results are described for one of the 15 fields (field C1), because all fields show more or less similar results and the results of the field that is described here are considered to be representative for all fields. In Appendix 5, results are shown for all 15 fields.

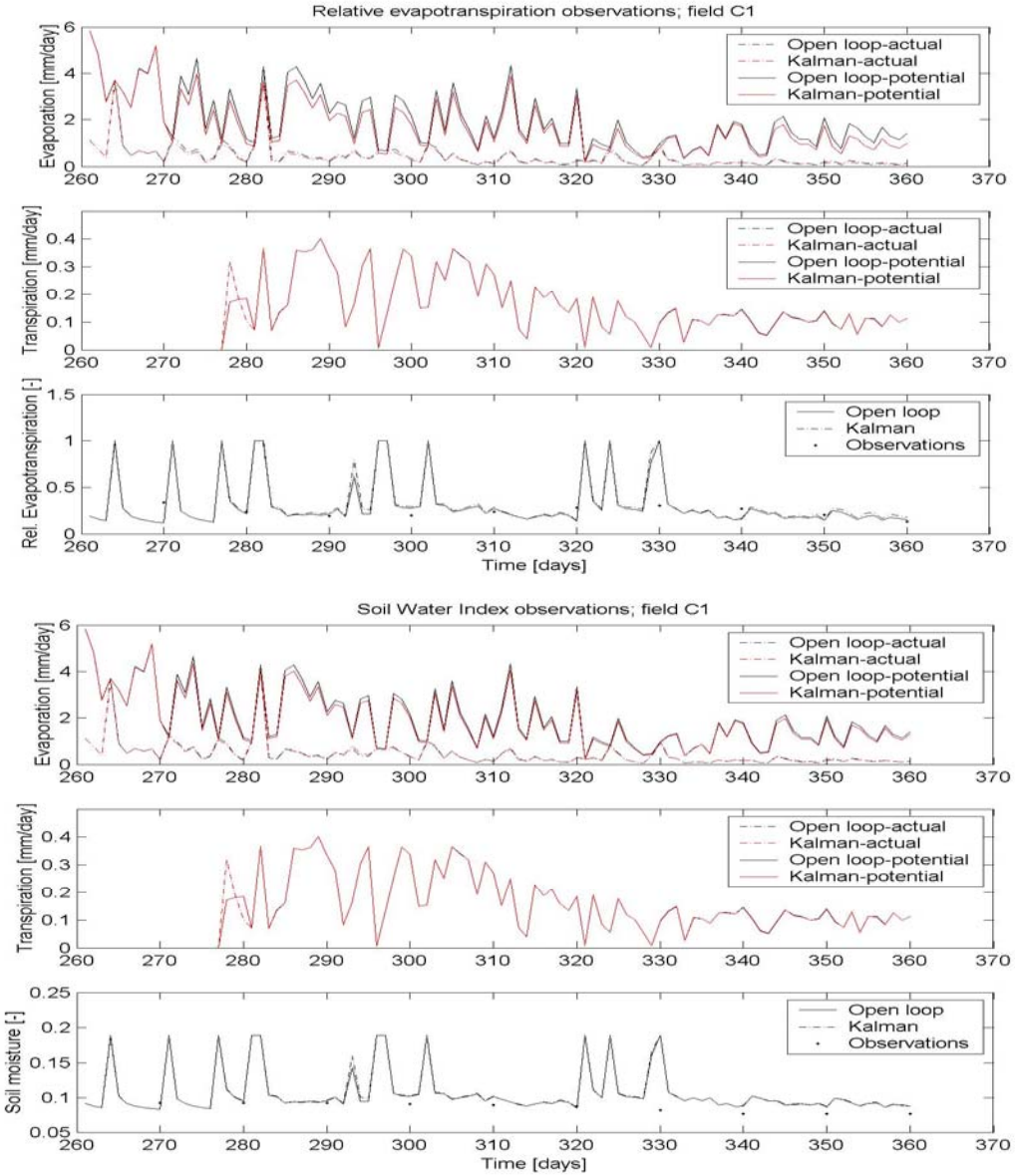

Figure 4-4 Modeled fluxes with and without the Kalman filtering, for one field (C1). In the upper three plots updating occurred with RET observations, in the lower three with SWI observations. For both observation types, from top to bottom: actual and potential evaporation, actual and potential transpiration and relative evapotranspiration (for RET observations) or soil moisture content (for SWI observations) respectively.

In Figure 4-4 the model output fluxes (actual and potential evaporation and transpiration), and the relative evapotranspiration and soil moisture content that were derived from them are shown, for an open loop simulation and a simulation with the Kalman filtering. It appears that the effect of the filtering was minimal, especially for the case with SWI observations the influence seemed negligible. The only significant effect of the Kalman filtering seemed to be on potential and actual evaporation, they were lowered slightly. This can be explained by the fact that the input variable of the

model that is re-initialized by the Kalman filter was the initial soil moisture content, which mainly influences evaporation.

Some important factors in the use of the Kalman filter are the choice of the ensembles, and the value B that was used. As already explained in Section 4.3, a value of 1 was assumed for B. In an attempt to enlarge the effect of the updating, a value of 2 for B was used as well. Results for this can be found in Table 4, where root mean square errors (RMSE) are given for the two values of B. The RMSE was calculated according to Equation (4-9):

$$RMSE = \sqrt{\frac{1}{N}\sum_{i=1}^{N}(sim_i - obs_i)^2} \qquad (4\text{-}9)$$

in which N is the number of observation times and simi and obsi are the model simulation and observation at each observation time respectively. As can be seen in Table 4, the difference between the control run and Kalman filtering run was low, and the increased B hardly made any difference.

In Table 4, and also in Figure 4-4, it appears that although observed values tend to be lower than modeled ones, the runs with Kalman filtering appear to be slightly higher. As appears from Figure 4-4, the changed soil moisture content mainly affects potential evaporation in the model, which has a negative effect on the relative evapotranspiration and soil moisture content. Therefore the difference with observations slightly increases and even more using a higher value for B. When the model is updated using SWI observations, the effects were smaller than using RET observations, this was probably because the modeled relative evapotranspiration had to be converted to soil moisture content before updating, taking away some of the ensemble variability because the numbers are smaller (a range of 0.05 - 0.2 for soil moisture, compared to 0.1-1.0 for RET). Besides, as can be seen in Figure 4-7, over the whole period, soil moisture derived from SWI observations was closer to modeled soil moisture as RTP observations were to modeled relative evapotranspiration, leading to less distinct changes for SWI observations.

In Figure 4-5 the again all modeled fluxes are shown, but instead of the ensemble averages now all ensemble members are plotted. Again, the main effect of the variance caused by the ensemble is visible in the evaporation plots, and then only in parts of the simulation period. This has also to do with the composition of the ensemble (see Table 4), in which mainly variables that were supposed to have an important effect on the state variable (soil moisture) were varied, i.e. rainfall, temperature and initial soil moisture content. Even though the range in values for the ensemble members was quite large, the effect in variability on the resulting relative evapotranspiration was relatively low.

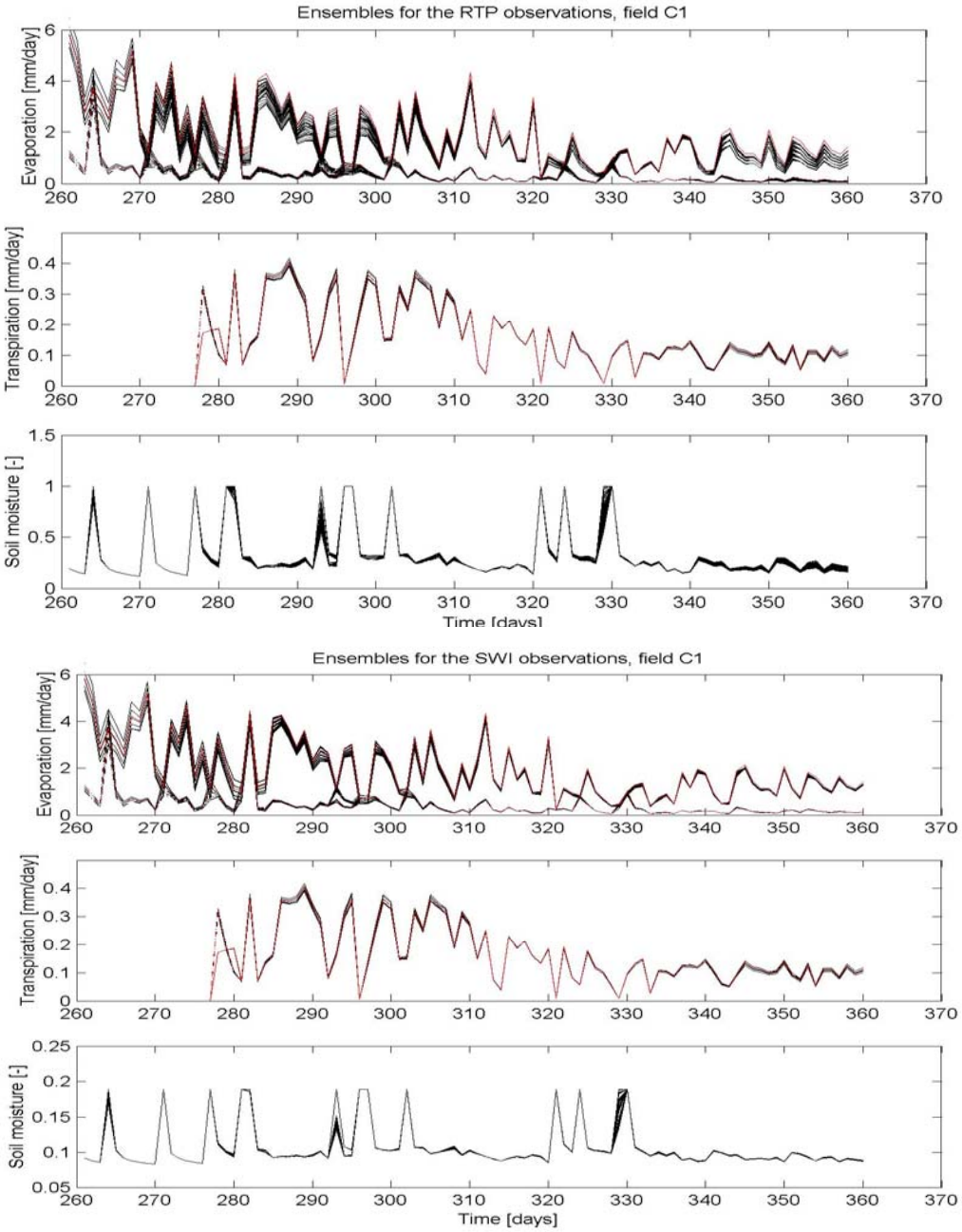

Figure 4-5 Same as Figure 4-4, but instead of ensemble averages here all ensemble members are shown. The red line is the case without Kalman filtering.

Table 4 Root mean square errors for field C1, for RET and SWI observations and two different values of B.

	Control	**B=1**	**B=2**
RTP	0.240492	0.241473	0.241620
SWI	0.034879	0.034987	0.035000

Figure 4-6 shows the root mean square error of each ensemble member with respect to the open loop simulation, which was calculated for according to Equation (4-10):

$$RMSE = \sqrt{\frac{1}{N}\sum_{i=1}^{N}(member_i - control_i)^2} \qquad (4\text{-}10)$$

where N is the number of days, and memberi and controli are the state variable value of the ensemble member and the corresponding value of the open loop run respectively. The way the ensemble is composed is as follows: five values are assigned to each of the three variables; the first 25 members use the lowest value of initial soil moisture content, of which the first 5 have the lowest value of precipitation and have 5 different values for temperature. The next 25 members correspond to the one but lowest value of soil moisture of which numbers 6 to 10 have the one but lowest value for precipitation and 5 different values for temperature, and so on.

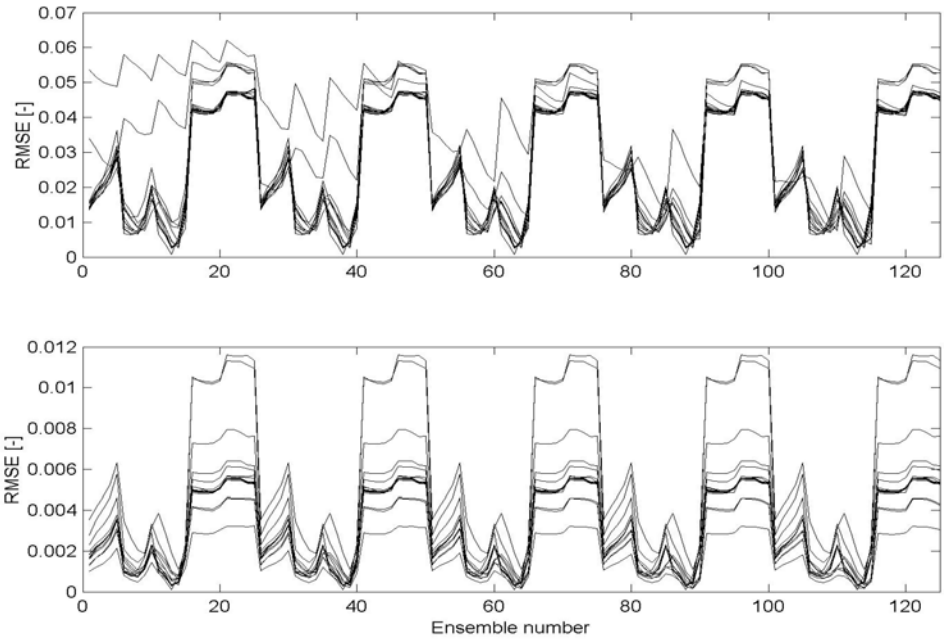

Figure 4-6 Root mean square difference (averaged over time) between the control run and the 125 ensemble members for all fields, for RET (upper plot) and SWI (lower plot) observations.

What can be seen from Figure 4-6 is the effect of each of the three variables on the eventual variability within the ensemble. What strikes first are the five high peaks, with a width of about 10 members. They correspond to the two highest values of precipitation. This variable, and especially its higher values, had thus a large impact on the result. Further, it appears that the pattern over the first 25 ensembles repeats itself 5 times, without any significant changes. This indicates that the initial soil moisture content had hardly any influence at all, which explains the low impact of the Kalman filter, since initial soil moisture content was the variable that was updated

after each observation. Apparently, the model was rather insensitive to input soil moisture content. Also temperature caused significant variability, causing the peaks that occur about every 5 members, albeit not as distinct as the peaks caused by precipitation.

To illustrate the functioning of the Kalman filter, in Figure 4-7 the modeled, observed and updated relative evapotranspiration or soil moisture content (depending on the type of observation) are shown. The observed and updated variables were only available every 10 days, so the plots are on a 10 day base. Also the result of the run with a B-value of 2 is shown. Here it appears that the modeled RET or soil moisture was forced to the observations and changed significantly. Also the difference between the two values for B can be seen clearly: updating occurs more distinctly. Since the updated soil moisture content was used to reinitialize the model, and still the model output hardly changed, it again appears that the model was rather insensitive to the input soil moisture content.

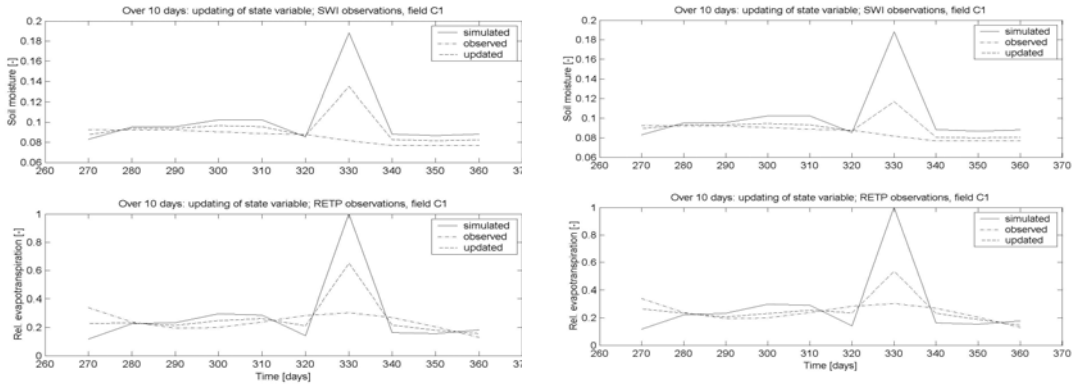

Figure 4-7 Updating of the model with the observations for two values of B: left B=1, right B=2. In the upper plots SWI observations were used, in the lower plots RET observations. At each updating time, the simulated, observed and updated values are shown. Since this occurs only 10 times during the period, the plots are in 10-day stretches.

4.5 Discussion

From the results that were described before, some issues arose that influenced the results. In this section those issues will be described and discussed.

Firstly, there was the adjustment of the crop growth model, Rotask 1.5. Since the model was developed for simulating a whole growing season, it had to be changed here to make it suitable for application with the EnKF. This meant the model had to be able to run in pieces between observations. Since in one of the observation datasets that were available here observations were available at a daily base, the model should be able to run at one day at a time. However, since other observation data was available every 10 days, and many technical problems occurred with the model running from day to day, it was decided to run the model at pieces of 10 day at a time (Figure 4-2). Although in this case results were better than for the day-to-

day case, they are not perfect yet: there are still problems with re-initializing the crop state variables at the start of every new stretch, and they synchronization of the various model routines.

A second topic is the selected dataset of observations. It proved to be hard to find observation datasets that were suitable for this case. Since the model operated at field scale, ideally field measurements or very high-resolution remotely sensed measurements should be used. It's questionable whether the large scale satellite estimations that were used here were representative for the fields under consideration.

Also the temporal scale appeared to be difficult; for example the relative evapotranspiration observations had to be interpolated over time (and space), due to cloud cover there were not enough actual measurements to use. Due to this interpolation, the rainfall peaks that show up very clearly in the simulations were smoothed and not visible in the observations. Therefore it is questionable whether it is right to update the detailed simulation information with observed data where important information is 'smoothed' out; this also holds for the SWI observations that were only available at a 10 day base.

A more general disadvantage of the EnKF is the rather arbitrary Kalman gain, which as appears from this study, plays an essential role in the algorithm. Theoretically it is possible to quantify this Kalman gain: it is a function of the covariances of the errors in model and observations, as is explained in section 4.2.2. Without additional field measurements it is not possible to quantify the error covariance in model and observations, so a value has to be estimated or taken from literature. In such situations this has to be done with great care, but in any case this remains an arbitrary and sensitive part of the EnKF.

Another factor that was the case in this particular application of the EnKF was in the fact that the state variable to be updated was in one of the cases relative evapotranspiration, while the crop growth model does not directly compute that quantity. The only related variable it can be initialized with is soil moisture content. Here relative evapotranspiration is assumed equal to relative soil moisture content, and by means of soil data (soil moisture contents at field capacity and wilting point) subsequently actual soil moisture content is calculated. According to Su et al., 2003 this assumption is valid, but only when soil moisture content is the limiting factor of evapotranspiration, in the case of potential evapotranspiration the relative soil moisture content can be higher than relative evapotranspiration. Therefore, in some periods during the simulation this assumption may have introduced an error in the result, although, according to Su et al., 2003, this error is relatively small.

4.6 Conclusions and Recommendations

In general, data assimilation and Kalman filtering can improve model results, if a proper model and suitable observations are used. With the model that was used in this work, there was no clear state variable to assimilate: soil moisture was the only

input variable related to the observations, while the model output consisted of fluxes such as relative and actual evapotranspiration. To convert these fluxes to soil moisture in order to be able to reinitialize the model various assumptions were needed and possibly errors were introduced. Besides, as was already described, the model turned out to be rather insensitive to changes in the initial soil moisture, since changes in output were minimal. Still, the EnKF itself was able to force simulated variables towards observed ones (Figure 4-6), however because of the factors described above this did not explicitly appear in the results. Apart from the model, that was not altogether suitable for application with the EnKF, it also turned out to be hard to find suitable datasets, due to both spatial and temporal scale problems, as was described before, in the discussion.

The first recommendation that can be made is to look further into how to adjust the crop growth model: to make it run in small time periods properly. Also it might be worthwhile trying to use an altogether different model, which is easier to adjust or already configured for simulating small periods at a time. A second improvement would be in the observation datasets: the output generated by the model contained far more details (both spatial and temporal) than the observation datasets; e.g. the reaction of soil moisture to rainfall events was smoothed out in the observations. An observation dataset should be found or created containing daily, high resolution (ideally field scale) measurements. Lastly, the Kalman gain is very important to the EnKF and also very arbitrarily, if no additional information about errors are available. By comparing both model and observations (of different kinds) to the results of field experiments information could be obtained about errors and error variances in both model and observations. If such information is known, the value of the Kalman gain can be derived much more easily.

5 Drought Risk Reduction in the Sudano Sahel of West Africa

(Ir. R.E.E. Jongschaap, Ir. S. Dione, Dr. A.L.Smit, Ir. M. Paganini)

5.1 Introduction

The project Drought Risk Reduction in the Sudano Sahel of West Africa was executed in combination with the Climag West Africa project; a network project supported by the European Commission (Contract n°: EVK2-CT-2000-80001), under the Energy Environment and Sustainable Development research programme, and by the START International Secretariat, within the framework of the Climate Prediction and Agriculture programme.

Increasing climate-mediated food insecurity and natural resource degradation is among the most pressing global change issue in West Africa. Improved management of the impacts of climate fluctuations on agro-ecosystems at the farm scale is one of the most important potential adaptations to anticipated global change.

The project enables and evaluates the practical application of emerging capacity to predict climate fluctuations and associate food production risks to improved management of agro-ecosystems. This will be accomplished through a systems

approach that links and integrates various components of existing knowledge in several fields including climate modelling and prediction, agro-ecosystem simulation and analysis, and ecological scaling theory.

In this framework, Mali has been designated as a test area in West Africa. The choice of Mali is justified by the institutional conditions, which allow an effective implementation of a demonstration project. The results and recommendations coming from the project should be applicable in the whole Sahel region. The project wants to verify the potential value of forecasts of inter-annual climate fluctuations for improving food crop production and thereby reducing risk for farmers with different kind of resources. The project is also addressed to enhance the interactions among end-users concerned with the consequences of climate variability on food security and natural resource management in the region and improve local climate prediction skill by specific training.

The focuss of the work is on "Agro-ecosystem modelling and analysis". The objectives are the application of Early Warning for crop modeling and the application of crop modelling for agriculture strategies assessment (Maracchi et al., 2001).

5.2 Project organization

5.2.1 Capacity building and knowledge transfer

The work of a trainee-ship and knowledge transfer between *Plant Research International* from the Netherlands (PRI) and the *Institut d'Economie Rurale* (IER) from Mali contributes to the objectives of the Drought Risk Reduction project. A training workshop was organized at *IER* in Bamako (Mali) by *Plant Research International.*

In the workshop, the simulation model CP-BKF3 was introduced to a group of scientists and extension workers. The training of the *IER* scientist at *Plant Research International* in Wageningen (the Netherlands) took place from September to December 2002. This training aimed to validate the CP-BKF3 model for yield predictions in Mali, for three major crops: sorghum millet and maize. The validation work involved available historical production data and the comparison of the results obtained by simulation to the FAO and national statistical values for the demonstration areas.

The training also focused on the simulation of crop production and nutrient efficiency for different regions, different soil types, and different farm types to demonstrate the effect of different climatic conditions. Therefore, 20 years of historical weather data were analyzed in scenarios. These scenarios help to understand how the changes of seasonal parameters, of soil type and of the farmer type affect the model crop production simulation results.

5.2.2 CP-BKF3 simulation model

The simulation model CP-BKF (Cultures Pluviales-Burkina Faso) has been built based upon preceding models by Van Kraalingen and Van Keulen (1988), Van Duivenboden and Cissé (1989) and Erenstein (1990). The model evolved stepwise. CP-BKF1 was firstly developed in 1994 to describe sorghum plant growth related to water availability as the only reacting factor. The CP-BKF2 followed the same year but involved beside sorghum, the millet and maize crop grown under rain-fed conditions. The lastly developed version is the CP-BKF3 model that integrates nitrogen and water as growth factors of sorghum, millet and maize. More details of CP-BKF3 can be found in Verberne *et al.* (1995). Model use and model processes are presented in this report.

CP-BKF3 is based on mechanistic relations between crop performance and environmental conditions such as climate and soil. The model handles cereal growth at three levels: 1) not limited, 2) water limited and 3) water and nitrogen limited. It simulates dry matter production and partitioning in a pest-, disease- and weed-free environment. The water module is based on tipping-bucket principles extended with water redistribution by capillary rise. Other processes account for emergence, evapo-(transpi)-ration, maintenance, root distribution and extension, development and death of plant organs, N fertilization, N uptake, N mineraliza-tion and immobilization, N leaching, run off, and drainage. Management practices include fertilization (type, quantity and split dose), ploughing and the construction of borders and ridges to increase water storage. The model has a user-friendly interface (Figure 5-1), which allows parameter change in rerun files and scenario studies over a continued or discontinued period of 15 years. Rotation of crops is an option in rerun files.

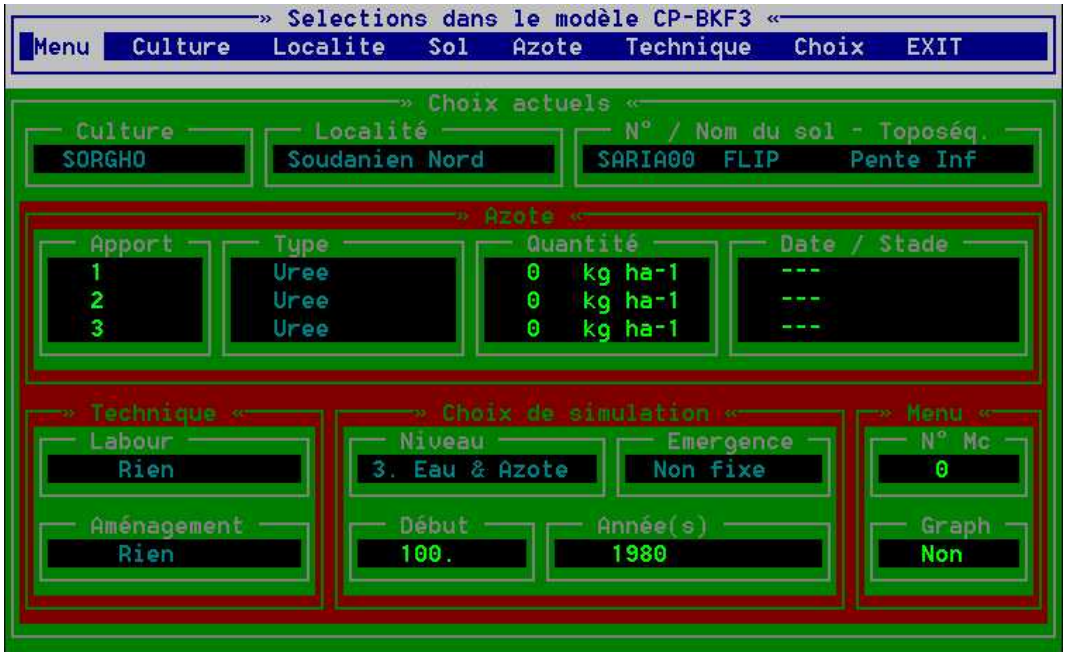

Figure 5-1Interactive screen of the CP-BKF3 simulation model

5.2.3 Field trials and literature research

With financial aid of *Plant Research International*, field experiments were conducted in Mali, in three different agro-cecological zones and cropping areas (Table 5; Palutikof et al., 2002). *IER* selected the villages Cinzana (5.99 E, 13.24 N) for millet experiments, Konobougou (6.80 E, lat. 12.25 N) for sorghum experiments, and Diou (5.97 E, 10.59 N) for maize experiments.

Table 5 Synoptic stations in three agro-climatic zones in Mali

Zone 1	Zone 2	Zone 3
Bamako	Kita	Hombori
Bougouni	San	Mopti
Koutiala	Segou	Nara
Kikasso		

Konobougou and Cinzana are two villages of the region of Segou. In both villages millet and sorghum are grown, but the village of Cinzana is known to have more millet than sorghum production, while for Konobougou the contrary is true. Diou is located in the far south of Mali, near the Ivory cost border. Diou is one of the districts of the Sikasso region. The main crop grown in this area is maize. However, the farmers at this location grow many other crops, such as cotton, rice tubers and vegetables.

With 3 crop types (millet, sorghum and maize) and 3 locations in each agro-ecological zone, 3 farmer types (A, B, C) per location, two fertilization application scenarios (0 and 100 kg complex fertilizer) and 5 harvest dates, an experimental set-up was designed (Table 6).

Table 6 Experimental set-up, number of samplings and number of harvested plants

Fertilization	Samplings				
Number	1	2	3	4	5
Date	16-Jun-'02	16-Jul-'02	5-Aug-'02	25-Aug-'02	16-Sep-'02
Harvested plants	20	20	10	5	5

At harvest dates, the whole fresh plant sample was weighed (see number of harvested plants in Table 6). Then the individual plant parts (roots, stems, leaves and cobs/grains) were weighed separately. Row distances were noted, and the number of plants in a 10 m row were counted (in 3 replicates) to establish plant density. Counting the plants was done at every harvest, to account for the thinning practice. Thinning is done to reduce the number of plants per sow pit, when sowing rates were too high (too many seeds per plant hole). A sample of fresh leaves was taken, weighed again, and the width and length was recorded in order to establish the leaf area index (m^2 $plant^{-2}$).

The crop samples were sun-dried in Mali, and weighed again. A sub-sample was weighed and sent to the Netherlands to be analyzed at the Central Laboratory of the Wageningen University. The samples were dried again at 70 ºC and analyzed for dry matter content and water content (Houba et al., 1997). Furthermore, the total

nitrogen content (N) was established by SFA, as were the total phosphorous (P) content at SFA and total potassium content (K) by flame AES (Temminghoff et al., 2000).

5.2.4 Data collection

Twenty years of precipitation data (1961-1980) were collected for 12 meteorological stations throughout Mali to enable model validation. General soil data were collected and soil characteristics for different agro-ecological zones in Mali were retrieved (PIRT, 1983; Quak et al., 1993). Soil data were converted to simulation model entries. For model analysis, meteo data were assigned to 5 different classes based on the rainfall during the year (Table 7), and based on the rainfall during the growing season (Table 8). The classes were: very dry, dry, normal, wet and very wet.

Table 7 Meteo stations and climate data: deviation (%) from mean yearly precipitation value for 20 years. Five classes are indicated: very dry (orange), dry (white), normal (light green), wet (green) and very wet (dark green).

Years	Bougouni	Gao	Kayes	Kita	Mopti	Nioro-S	San	Segou	Sikasso	Hombori	Koutiala	Niono
1961	6	11	1	6	-15	2	13	6	-2	-8	-58	-47
1962	31	-23	-3	32	20	37	-2	14	-2	13	-43	-40
1963	17	50	35	-12	1	32	9	11	-1	4	35	-52
1964	27	50	5	12	29	47	18	32	7	5	89	-26
1965	-16	23	18	8	37	8	9	13	-16	-1	-43	-67
1966	8	-2	30	10	-14	26	2	6	6	-1	4	-54
1967	-7	-14	3	20	15	0	4	5	10	13	64	-20
1968	-22	-14	-26	4	-7	-9	6	-19	18	7	-55	63
1969	2	-2	23	-3	5	11	-22	0	6	0	32	75
1970	1	-2	-15	-13	26	-18	-21	0	7	-8	-60	115
1971	-3	-8	-9	-8	1	-31	6	-26	-32	-4	36	79
1972	-20	-14	-26	-16	-20	-10	11	-23	-13	-4	22	-58
1973	-26	-24	-14	-4	-33	-27	-21	-26	-32	-16	-65	-60
1974	-8	-32	4	-3	-16	-15	-13	-10	-8	-19	66	28
1975	-1	7	-8	-2	15	2	-10	21	6	38	23	-32
1976	9	-7	-8	16	5	0	-3	3	32	-13	50	-52
1977	-11	-3	-9	-15	-27	-39	11	-1	-5	-12	-62	-48
1978	7	10	13	-13	-15	-8	10	-3	10	-12	-62	110
1979	4	-5	-15	-20	-6	-8	-6	-4	10	22	30	84
1980	-1	60	-26	-21	24	-37	8	-26	7	-20	11	-48

Eventually, simulation results were analyzed based on the seasonal rainfall classification (Table 8). The five classes (a-e) were set (arbitrarily) to:

a) Very wet years, with rainfall between May 25th and October 1st, differing +30% and more, compared to average rainfall
b) Wet years, with rainfall between May 25th and October 1st, differing between +10% and +30%, compared to average rainfall
c) Normal years, with rainfall between May 25th and October 1st, differing between -10% and +10%, compared to average rainfall
d) Dry years, with rainfall between May 25th and October 1st, differing between -10% and -30%, compared to average rainfall
e) Very dry years, with rainfall between May 25th and October 1st, differing -30% and more, compared to average rainfall

Table 8 Meteo stations and climate data: deviation (%) from mean season precipitation value (May 25th-October 1st) for 20 years. Five classes are indicated: very dry (orange), dry (white), normal (light green), wet (green) and very wet (dark green).

Years	Bougouni	Gao	Kayes	Kita	Mopti	Nioro-S	San	Segou	Sikasso	Hombori	Koutiala	Nioro
1961	0	12	6	14	-16	11	17	15	9	-3	-58	-50
1962	3	-20	-8	27	18	44	-1	14	5	20	-50	-38
1963	0	39	34	-24	-17	25	2	-5	-7	-1	30	-53
1964	-4	53	14	15	28	58	24	38	18	11	96	-32
1965	-20	28	20	18	35	15	19	25	-13	7	-44	-62
1966	2	-2	32	-2	-19	16	0	11	13	7	10	-51
1967	-3	-9	11	26	15	9	11	14	9	18	73	-16
1968	-20	-9	-26	5	-3	-4	7	-19	14	12	-59	70
1969	-26	0	0	-3	9	12	-20	-1	2	-6	32	70
1970	4	0	-6	-7	32	-9	-20	8	13	-13	-62	139
1971	17	-4	0	2	3	-28	4	-28	-29	4	50	89
1972	4	-13	-24	-13	-25	-11	7	-23	-13	4	16	-58
1973	-16	-21	-11	2	-36	-27	-21	-27	-29	-10	-62	-57
1974	-9	-31	9	5	-20	-9	-7	-1	0	-12	70	38
1975	3	-30	-6	2	15	-2	-19	20	6	42	27	-37
1976	-11	-10	-6	-3	5	-2	-13	-12	20	-33	15	-55
1977	21	1	-2	-10	-25	-42	7	7	-4	-13	-63	-43
1978	4	-28	10	-18	-23	-11	3	-4	-12	-13	-63	121
1979	31	-21	-23	-25	-10	-12	-13	-10	-12	5	26	68
1980	20	67	-21	-13	34	-33	14	-19	10	-23	17	-43

5.3 Simulation experiment

The simulation was set with the factors that may affect crop growth and yield production in the Soudano Sahel region: farmer type (reflecting farm management possibilities), soil type, slope, field management techniques and the use of inorganic fertilizer (Table 9).

It was assumed that all farmers had the posibility to choose the position of their fields: on plateaus, on slopes or in the valleys, thereby following the natural gradient of soil moisture availability caused by increased soil fertility and run-off, as found in such toposequences.

These factors were tested under different weather conditions, by simulating 20 years of weather data (1961-1980), in order to identify the effects of dry and wet years for the selected farming systems. Data were analysed according to a completely randomised design with Restricted Maximum Likelihood (REML) using the statistical software package Genstat (2002).

Table 9 Farmer type characterization for model simulations. From A to B to C, farmers have fewer options to adapt to manage their fields

	A-type farmer	B-type farmer	C-type farmer
Soil types and location	All	All	All
Slope	0-5 degrees	0-5 degrees	0-5 degrees
Application of organic waste	15000 kg ha^{-1}	7500 kg ha^{-1}	3750 kg ha^{-1}
Fertilizer Use	0, 50, 100 urea kg ha^{-1}	0, 50 urea kg ha^{-1}	0 urea kg ha^{-1}
Effective ploughing	10 cm (animal plough)	5 cm (hand plough)	1 cm (raking)
Soil water conservation method	Furrows + Contour ridging	Countour ridging	(nothing)

Fertilisation is an important choice for A- and B-type farmers. A-type farmers are more inclined to apply high doses than B-type farmers, whereas C-type farmers have no resources to pay for fertiliser at all. Accessibility to fertiliser has other constraints, such as access to markets and banks. The application of fertilisers introduces an extra risk for farmers, but fertilisation may pay off in normal, wet or very-wet seasons.

Ploughing is done, but ploughing method varies per farmer type. C-type farmers may only rake their fields (1 cm deep), while B-type farmers may use hand ploughs (5 cm deep) and A-type farmers may use animal traction (10 cm deep).
Soil water conservation methods are not practised by C-type farmers, whereas B-type farmers may include contour ridging and A-type farmers may integrate contour riding with special techniques for extra soil water conservation.

5.4 Results

5.4.1 Field trials

Field trials were laid out and executed in three agro-ecological zones in Mali. Analyses of these experiments were never fully completed, due to local problems with field observations (technical assistance and/or equipment was lacking) and with problems of getting subsamples to the Netherlands for chemical analyses. The partial datasets (Appendix 5 and Appendix 6) could not be used for full model calibration. Therefore additional literature research was needed to get supplementary data.

5.4.2 Model validation

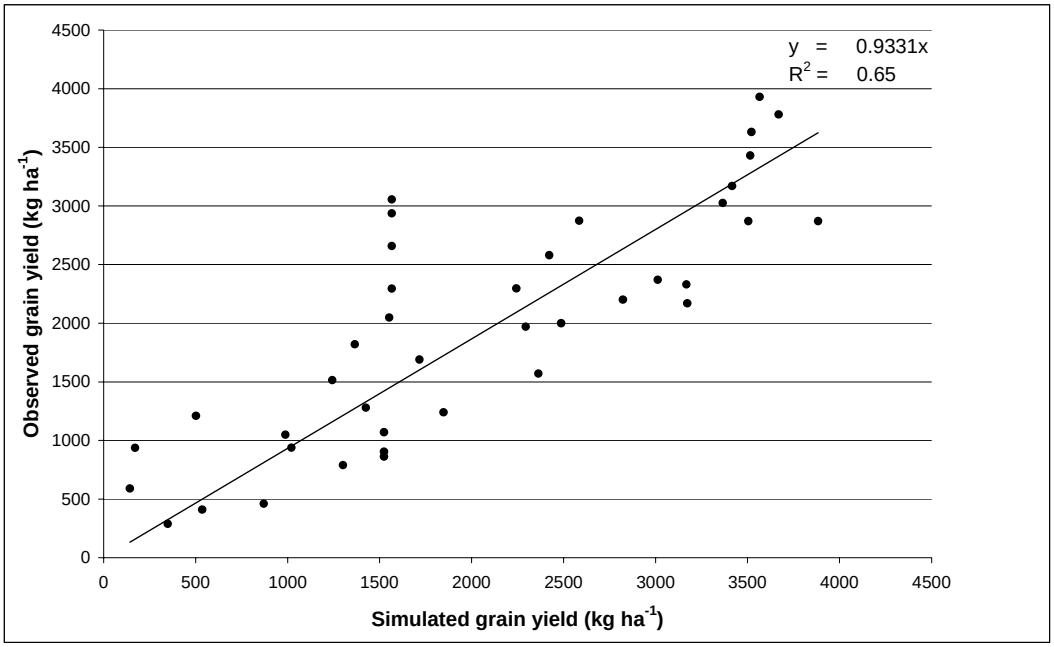

Figure 5-2CP-BKF3 model validation results: simulated vs. observed grain yield (kg ha-1) for millet, sorghum and maize for different locations in the Sudano Sahel region

After calibrating the simulation model on field experiments in Burkina Faso and on the partial datasets of Mali, the model was validated in the Sudano Sahel by using field observations from literature (Figure 5-2). These field observations comprised data from different crops (millet, sorghum and maize), in different agro-ecological zones with concurrent cropping system and with differences in crop management (cultivar, fertilizer, field preparations).

Simulation results gave satisfactory results, considering the fact that most experiment descriptions did not mention all necessary input data for the simulation model, and that climatic data was generally not recorded at the site but had to be taken from nearby synoptic stations. Where data was lacking, expert knowledge was introduced. It was concluded that the model would be a valuable tool for further analysis of climate prediction and adaptation strategies of farmers in the Sudano Sahel region.

5.4.3 Model execution, output and statistical analysis

The settings for A-, B- and C-type farmers, combined with the environmental settings and the climate records, resulted in 67200 model runs (A: 38400 runs, B: 25600 runs and C: 3200 runs). The model did not report any anomalies during execution, nor did the outcomes raise attention to specific problems. In some simulation years and for some combination of factors, the simulation model gave notice of crop failure. These outcomes coincide with real time observations in Mali, such as the dry spells in 1973 and 1979.

A selection of possible outputs was requested from the simulation model, as model output can be tailored to ones needs (Table 10). From these selected output variables, Dry weight of grain (WGR), Nitrogen in areal biomass (NMBA) and Water use efficiency (WUE) were taken for further analysis.

Table 10 Simulation output variables and calculated variables of CP-BKF3 simulation model

Variable	Unit	Explanation
Direct output		
TIME	(Julian day number)	Day of year that simulation stopped
EMDOY	(Julian day number)	Emergence day of year
WGR	(kg ha^{-1})	Dry weight of grain
WSHTOT	(kg ha^{-1})	Dry weight of aerial biomass
NBMA	(kg ha^{-1})	Total nitrogen in aerial biomass
TRAIN	(mm)	Total precipitation
TERAIN	(mm)	Total effective precipitation
TDRAIN	(mm)	Total seepage/drainage
TLEACH	(kg ha^{-1})	Total nitrogen leaching
Calculated output		
LGP	(days)	Length of growth period = TIME - EMDOY
HI	(kg kg^{-1})	Harvest Index = WGR / WSHTOT
NitEff	(kg N kg^{-1} N_0)	Nitrogen efficiency = NBMA / Nfert (N_0 = 0 scenario)
PrecEff	(mm mm^{-1})	Precipitation efficiency = TERAIN / TRAIN
WUE	(kg DS kg H_20)	Water Use Efficiency = (WGR * 1.E3) / (TERAIN * 10.E3)

5.4.4 Farmer type and crops

Grain weight production (kg ha^{-1}) differed signifficantly (P<0.01) between farmer types over all climate situations and environmental settings (Table 11). Average values for millet were 368 kg ha^{-1} for A farmers, 337 kg ha^{-1} for B farmers and 273 kg ha^{-1} for C farmers. Average values for sorghum were 1099 kg ha^{-1} for A farmers, 983 kg ha^{-1} for B farmers and 796 kg ha^{-1} for C farmers. Average values for maize were 2086 kg ha^{-1} for A farmers, 1674 kg ha^{-1} for B farmers and 1255 kg ha^{-1} for C farmers. Effects of single factors and 2-way interactions are discussed per crop.

Table 11 Grain weight production (kg ha^{-1}). Average values per farm-type (A, B and C) over all environmental settings (region, soil type, slope, field position on topographic position and management options). Values in columns, with different letters (A, B, C, D and E) differ significantly (P<0.01) and values in rows (per crop) with different small letters (a, b and c) differ significantly (P<0.01).

Climate	Millet			Sorghum			Maize		
Qualification	A	B	C	A	B	C	A	B	C
Very dry	19^{Aa}	27^{Aa}	21^{Aa}	64^{Aa}	81^{Aa}	112^{Aa}	469^{Aa}	343^{Aa}	291^{Aa}
Dry	135^{Ba}	134^{Ba}	121^{Ba}	914^{Ba}	842^{Bb}	699^{Bc}	2276^{Ba}	1854^{Bb}	1382^{Bc}
Normal	258^{Ca}	251^{Ca}	225^{Ca}	1271^{Ca}	1144^{Cb}	923^{Cc}	2550^{Ca}	2054^{Cb}	1532^{Cc}
Wet	539^{Da}	504^{Da}	404^{Db}	1494^{Da}	1317^{Db}	1064^{Dc}	2347^{Da}	1907^{Db}	1459^{Cc}
Very wet	890^{Ea}	770^{Eb}	597^{Ec}	1749^{Ea}	1530^{Eb}	1181^{Dc}	2788^{Ea}	2211^{Eb}	1611^{Cc}

Millet

For single factors, only plough type made no significant difference for millet grain production. For 2-way interactions with climate, plough type, field position, slope and soil water conservation method made no significant difference for millet grain production. Only the interaction with nitrogen fertilisation was significantly different (P=0.002) There was no 2-way interactions with farm type other than with climate (P<0.001) for millet grain production. For 2-way interactions with nitrogen fertilisation, there was no significant difference for millet grain production. For 2-way interactions with slope, only soil water conservation method made significant difference for millet grain production (P<0.001).

Sorghum

The single factors climate, farm type, nitrogen fertilisation, field position, slope and soil water conservation method all made significant difference for sorghum grain production (P<0.001). Plough type was the only single factor that was not significant. For 2-way interactions with climate, only field position made significant difference for sorghum grain production (P<0.001).

Maize

The single factors climate, farm type, plough type and nitrogen fertilisation made significant difference for maize grain production (P<0.001). Less significant were the factors slope (P=0.01) and soil water conservation method (P=0.05) Field position was the only single factor that was not significant. For 2-way interactions with climate, field position significant difference for maize grain production (P<0.001). Less significant were nitrogen fertilisation (P=0.004), slope (P=0.003) and soil water conservation method (P=0.002). Not significant was plough type. For 2-way

interactions with farm type, only field position, plough type and slope were not significantly different (P<0.001) for maize grain production. For 2-way interactions with nitrogen fertilisation, there was no significant difference for maize grain production. For 2-way interactions with plough type, there was no significant difference for maize grain production. For 2-way interactions with slope, there was no significant difference for maize grain production. For 2-way interactions with soil water conservation method, there was no significant difference for maize grain production.

5.4.5 Nitrogen uptake

Nitrogen uptake in aerial biomass was produced by the simulation model as kg N ha^{-1}. The climatic effects of fertilization efficiency are summarized in Table 12. Effects of single factors and 2-way interactions are discussed per crop.

Millet
For single factors, only plough type made no significant difference for nitrogen uptake. All other factors were significant at P<0.001 level. For 2-way interactions with climate, nitrogen fertilisation (P<0.001), slope (P=0.011) and soil water conservation method (P=0.004) made significant difference for nitrogen uptake. There was no 2-way interactions with farm type other than for climate (P<0.001) for nitrogen uptake. For 2-way interactions with nitrogen fertilisation, there was no significant difference for nitrogen uptake. For 2-way interactions with plough type, there was no significant difference for nitrogen uptake. For 2-way interactions with slope, there was no significant difference for nitrogen uptake. For 2-way interactions with soil water conservation method, there was no significant difference for nitrogen uptake.

Sorghum
All single factors climate, farm type, field position, nitrogen fertilisation, plough type, slope and soil water conservation method made significant difference for nitrogen uptake (P<0.001). For 2-way interactions with climate, nitrogen fertilisation (P<0.001) and field position (P=0.037) made significant difference for nitrogen uptake (P<0.001). For 2-way interactions with farm type, climate, field position and nitrogen fertilisation were significantly different (P<0.001) for nitrogen uptake.
For 2-way interactions with nitrogen fertilisation, field position was significant difference for nitrogen uptake (P=0.012). For 2-way interactions with plough type, nitrogen fertilisation was significant for nitrogen uptake (P<0.038). For 2-way interactions with slope, there was no significant difference for nitrogen uptake (P<0.001). For 2-way interactions with soil water conservation method, plough type made significant difference for nitrogen uptake (P<0.019).

Maize
All single factors climate, farm type, nitrogen fertilisation, field position, plough type, slope and soil water conservation method made significant difference for nitrogen uptake (P<0.001). Plough type was the only single factor that was not significant. For 2-way interactions with climate, all factors made significant difference for nitrogen

uptake (P<0.001), with the exception of plough type. For 2-way interactions with farm type, only climate and nitrogen fertilisation were significantly different (P<0.001) for nitrogen uptake. For 2-way interactions with nitrogen fertilisation, no factor made significant difference for nitrogen uptake. For 2-way interactions with plough type, there was no significant difference for nitrogen uptake (P<0.001).
For 2-way interactions with slope, there was no significant difference for nitrogen uptake (P<0.001). For 2-way interactions with soil water conservation method, slope made significant difference for nitrogen uptake (P=0.019).

Table 12 Grain weight production (kg ha^{-1}) as result of 0, 50 and 100 kg urea ha^{-1} (45% N) averaged over all farmer types (A, B and C). Values in columns, with different letters (A, B, C, D and E) differ significantly (P<0.01) and values in rows (per crop) with different small letters (a, b and c) differ significantly (P<0.01).

Climate	Millet			Sorghum			Maize		
Qualification	0	50	100	0	50	100	0	50	100
Very dry	22^{Aa}	22^{Aa}	22^{Aa}	85^{Aa}	86^{Aa}	86^{Aa}	361^{Aa}	370^{Aa}	371^{Aa}
Dry	129^{Ba}	130^{Ba}	130^{Ba}	753^{Ba}	849^{Bb}	853^{Bb}	1622^{Bb}	1935^{Bbc}	1955^{Ac}
Normal	242^{Ca}	246^{Ca}	245^{Ca}	1002^{C}	1161^{Cb}	1174^{Cb}	1776^{Ba}	2164^{Cb}	2196^{Ab}
Wet	459Da	497^{Db}	492^{Db}	1188^{D}	1334^{Db}	1352^{Db}	1636^{BCa}	2022^{Db}	2054^{Ab}
Very wet	687^{Ea}	782^{Eb}	788^{Eb}	1382^{E}	1544^{Eb}	1533^{Eb}	1902Da	2343^{Eb}	2364^{Ab}

5.4.6 Water use efficiency

Water use efficiency was produced by the simulation model as g DM (grain) kg^{-1} H_2O. Dividing these values by 1000 (g kg^{-1}), and taking the inverse value, water use efficiency is expressed as: kg H_2O kg^{-1} DM grain. The significant effects of single factors and 2-way interaction on water use efficiency are discussed per crop.

Millet
For single factors, climate, farm type, field position and nitrogen fertilisation made significant difference for water use efficiency (P<0.001). For 2-way interactions with climate, nitrogen fertilisation made significant difference for water use efficiency (P=0.006). For 2-way interactions with farm type, climate (P<0.001), field position (P<0.001) and nitrogen fertilisation (P=0.003) made significant difference. For 2-way interactions with nitrogen fertilisation, there was no significant difference for water use efficiency. For 2-way interactions with plough type, there was no significant difference for water use efficiency. For 2-way interactions with slope, there was no significant difference for water use efficiency. For 2-way interactions with soil water conservation method, there was no significant difference for water use efficiency.

Sorghum
The single factors climate, farm type, field position, nitrogen fertilisation, and slope made significant difference for water use efficiency (P<0.001). Plough type and soil water conservation method made no significant difference for water use efficiency. For 2-way interactions with climate, only field position (P<0.001) made significant difference for water use efficiency (P<0.001), whereas nitrogen fertilisation was significant at P=0.054. For 2-way interactions with farm type, climate, field position and nitrogen fertilisation were significantly different (P<0.001) for water use

efficiency. For 2-way interactions with nitrogen fertilisation, no significant difference for water use efficiency was found. For 2-way interactions with plough type, there was no significant difference for water use efficiency. For 2-way interactions with slope, there was no significant difference for water use efficiency ($P<0.001$). For 2-way interactions with soil water conservation method, no significant difference for water use efficiency was found.

Maize

All single factors climate, farm type, nitrogen fertilisation, field position, plough type, slope and soil water conservation method made significant difference for water use efficiency ($P<0.001$). Plough type was the only single factor that was significant at $P=0.003$. For 2-way interactions with climate, no other factors made significant difference for water use efficiency ($P<0.001$). For 2-way interactions with farm type, only climate, nitrogen fertilisation and slope were significantly different at $P<0.001$. Field position was significantly different at $P=0.001$. For 2-way interactions with nitrogen fertilisation, only plough type made significant difference for water use efficiency ($P=0.003$). For 2-way interactions with plough type, there was no significant difference for water use efficiency ($P<0.001$). For 2-way interactions with slope, there was no significant difference for water use efficiency ($P<0.001$). For 2-way interactions with soil water conservation method, slope made significant difference for water use efficiency ($P=0.001$) and plough type was significantly different at $P=0.021$.

5.5 Discussion

The presented methodology for the analysis of climate adaptation strategies has shown what can be expected from a series of predefined adaptation techniques for farmers in the Sudano Sahel zone in different agro-ecological zones in Mali for grain growth. Of course: the simulation settings may be discussed and altered, but in the end a quantitative approach of available farmers' techniques (or new techniques!) can be evaluated against authentic environmental settings.

The simulated results show that farmers have ample possibilities within their cultural, social and economic packages to react upon forecasts for the coming growing season, and that these strategies may imply, e.g. increased or sustained grain production. The tables show what may be expected from all these adaptation strategies, in grain production, nitrogen uptake and water use efficiency.

If growing seasons can be characterised beforehand (i.e. before field preparations), and qualified as very dry, dry, normal, wet or very wet, farmers may calculate their risk and use other strategies to cope with this information. The method enables to scale farmers' decissions to higher integration scales, or higher administrative levels.

With the simulation model and some of the presented results can be calculated what the quantitative effects and risks would be, if adaptation strategies for a certain climate qualification type are applied, and if one of the other climate qualification type occurs.

The combination of adaptation stategies deserve specific attention, as has been shown that various 2-way interactions, including farm type and climate qualification, show significant differences between outcomes.

5.6 Conclusions

The methodology seems valuable for Early Warning Systems in the Sahel region, as more specific information from farmers' perspective and from environmental settings is taken into account. The model enables to upscale results from plot level to districts and regions, which makes forecasts under various scenarios most interesting.

Based on remote sensing and/or information stored in geographic information systems, the simulation model may be provided with more detailed information of ground truth (e.g. acreage of millet, sorghum and maize; start of growing season; field locations) in order to enhance early warning systems and the methodolgy that is presented here.

The economic consequences of farmers' strategies can be quantified, if outcomes in grain yield are subjected to (local) prices on markets, and the availability and prices of fertiliser. More restraints can be obtained by blocking access to fertiliser markets, or by investigating the closure of irrigation schemes.

6 Conclusions

The project has achieved to generate a prototype operational system to address the efficient use of water for sustainable food production and food security. Its operation can be realized without too much demand on specific knowledge that is only accessible to professionals. Particular attention is taken care by involving in the project besides research and education organizations also a Dutch commercial firm (SarVision) that is committed to providing operational remote sensing services. Part of the system has been implemented at the China Meteorological Centre in China in combination within its operational system.

Specifically, the main conclusions of the project can be summarized as follows:

The SEBS model has been implemented for the processing of NOAA/AVHRR and MODIS data and evaluation of the codes and the results against field observation data have been carried out. A time series of evaporation fraction images for a whole year is generated with the help of the HANTS algorithm using the results derived from the NOAA data. A time series of relative soil moisture is also generated similarly with the windscatterometer data. These results show that this part of the system is at a prototype stage and can be integrated in an operational environment.

Two retrieval algorithms for relative soil moisture using windscatterometer data are named the Wagner model and the Woodhouse model. Advantages and disadvantages of both methods are discussed. The retrieval algorithms of the two approaches are however considerably different. From the analyses it was difficult to compare both approaches. Although the Woodhouse model is a physically based scattering approach retrieval, the initialization was found to be cumbersome and produced a widely varying result, the Wagner model was preferred in this project because of its extensive testing and clear functionality. Given the range of validity of the Wagner model it is recommended that physically based models like that of Woodhouse et al be investigated further since they can cope with various surface characteristics that the Wagner model cannot in its current form. Validations of both algorithms using field observation data are needed before firm conclusion can be drawn.

The combination of remotely sensed environmental variables with a crop growth model in a data assimilation framework has been shown with the potential to improve prediction of drought events and consequences for crop yields. Two types of (indirect) observations were selected to be combined with the model simulation: firstly relative evapotranspiration was derived from NOAA/AVHRR data using the SEBS-model, secondly, from passive microwave remote sensing soil moisture content. To integrate observations and model simulation a data assimilation algorithm was selected using the sophisticated Ensemble Kalman Filter (EnKF)

The work that was executed in the Sudano Sahel part of the Drought Risk Reduction project included simulation experiments for adaptation strategies to forecasted

droughts or wet climate conditions. A valuable method for Agricultural Strategy Assessment and Early Warning Systems was achieved, by using crop growth simulation models (CP-BKF3), to quantify the effects of adaptation strategies in terms of agricultural production and resource use efficiency. The methodolgy seems valuable for Early Warning Systems in the Sahel region, as more specific information from farmers' perspective and from environmental settings is taken into account. The model enables to upscale results from plot level to districts and regions, which makes forecasts under various scenarios most interesting. Based on remote sensing and/or information stored in geographic information systems, the simulation model may be provided with more detailed information of ground truth (e.g. acreage of millet, sorghum and maize; start of growing season; field locations) in order to enhance early warning systems and the methodolgy that is presented here. The economic consequences of farmers' strategies can be quantified, if outcomes in grain yield are subjected to (local) prices on markets, and the availability and prices of fertiliser. More restraints can be obtained by blocking access to fertiliser markets, or by investigating the closure of irrigation schemes.

Overall, the project has generated a system that is shown potentially to be able to be used in monitoring, prediction and risk analysis of drought events. More specially the project has achieved the following aims: Increased capacity of scientist in China and Sudano-Sahel by means of technology transfer; Generation of a methodology to monitor drought and crop production risks.

References

Crow, W. T. and E. F. Wood, 2003, "The assimilation of remotely sensed soil brightness temperature imagery into a land surface model using Ensemble Kalman filtering: a case study based on ESTAR measurements during SGP97", Advances in Water Resources 26, 137-149.

Erenstein, O., 1990, "Simulation of water-limited yields of sorghum, millet and cowpea for the 5th region of Mali in the framework of quantitative land evaluation", CABO-DLO Report, Wageningen.

Evensen, G., 2003, "The Ensemble Kalman Filter: theoretical formulation and practical implementation", Ocean Dynamics 53, 343-367.

Genstat, 2002, "Genstat for Windows", Release 6.1, sixth edition, VSN International Ltd., Oxford.

Grippa, M. and I.H. Woodhouse, 2002, "Validation of Surface Scattering Models Across Large Footprints for Global Scatterometer Applications", IEEE Trans. Geoscience and Remote Sensing, Vol. 40, No. 10, 2229-2233.

Houba V.J.G., J.J. van der Lee and I. Novozamsky, 1997. Soil and plant analysis, part 5B. Syllabus Wageningen University, Wageningen, The Netherlands.

Jongschaap, R.E.E., 1996, "Rotask 1.0 – A dynamic simulation model for continuous cropping and tillage systems. Reference manual", Report 70, DLO Research Institute for Agrobiology and Soil Fertility, Haren, the Netherlands.

Jongschaap R.E.E. and S. Dione, 2004, "Model analysis of mitigation strategies tailored to climate variation forecasts", Plant Research International, Wageningen, the Netherlands. Internal report.

Kraalingen, D.W.G. van, and H. van Keulen, 1988, "Model development and application for the 'Project pilote en agrometeorologie", Report prepared for submission to World Meteorological Organization, CABO/TPE. Wageningen

Li, J., Z. Su, B. v.d. Hurk, M. Menenti, A. Moene, H.A.R. de Bruin, J.J. Baselga Yrisarry, M. Ibanez, A. Cuesta, 2003, "Estimation of sensible heat flux using the Surface Energy Balance System (SEBS) and ATSR measurements", Physics and Chemistry of the Earth 28, 75-88.

Loon, E. E. van and P. A. Troch, 2001, "Book of abstracts International workshop on catchment scale hydrologic modeling and data assimilation", Rapport 101, Wageningen University, the Netherlands.

Marracchi, G. (ed.), 2001 "CLIMAG-West Africa: a network for harmonisation of climate prediction for mitigation of global change impact in Sudano-Sahelian West Africa", Proceedings of an international workshop, Bamako, Mali, 23-25 April 2001, START/EU commission/FMA, Florence, Italy. 185 pp

Marrocu M. and C. Paniconi, 2001, "Assessment of data assimilation techniques for a 3D Richards equation-based hydrological model", technical report CRS4-TECH-REP-1/73, Center for Advanced Studies, Research and Development in Sardinia, Cagliari, Italy.

McLaughlin, D., 1995, "Recent developments in hydrologic data assimilation", U.S. National Report to International Union of Geodesy and Geophysics 1991-1994: Contributions in Hydrology, editors R. A. Pielke Sr. and R. M. Vogel, pages 977-984, American Geophysical Union, Washington, DC.

McLaughlin, D. B., 2002, "An integrated approach to hydrologic data assimilation: interpolation, smoothing, and filtering", Advances in Water Resources 25 (2002), 1275-1286.

Miller, R. N., M. Ghil and F. Gauthiez, 1994, "Advanced data assimilation in strongly nonlinear dynamical systems", Journal of Atmospheric Sciences 51, 1037-1056.

Oevelen, P.J. van, and I.H. Woodhouse, 1996, "NOPEX/FOREST-DYNAMO ground data collection and data analysis report".

Palutikof, J., D.Z. Diarra and T. Holt, 2002, "The CLIMAG methodology for seasonal forecasting in West Africa", Description and comparison with existing methologies WP2, deliverable 5.

Paniconi, C., M. Marrocu, M. Putti and M. Verbunt, 2003, "Newtonian nudging for a Richards equation-based distributed hydrological model", Advances in Water Resources 26(2), 161-178.

PIRT, 1983, "Projet d'Inventaire des Ressources Terrestre du Mali (USAID-technical report Vol II) ", TAMS, New York, 486 p.

Quak, W., H. Hengsdijk, E.J. Bakker, K. Sissoko and M. S. M. Touré, 1996, "Description Agronomique Quantitative Des Systèmes De Production Végétale En Zone Soudano-Sahelienne".

Rauwerda J., G.J. Roerink and Z. Su, 2002, "Estimation of evaporative fractions by the use of vegetation and soil component temperatures determined by means of dual-looking remote sensing", Alterra-report 580, ISSN 1566-7197, Centro for Geo-Information, Alterra Green World Research, Wageningen.

Reichle, R. H., D. B. McLaughlin and D. Entekhabi, 2002, "Hydrologic data assimilation with the Ensemble Kalman Filter", Monthly Weather Review, 130(1), 103-114.

Rodger, C.D., 1976, "Retrieval of Atmospheric Temperature and Composition from remote Measurements of Thermal Radiation", Rev. Geophys. Space Phys. Vol. 14, 609-624

Roerink, G. J. and M. Menenti, 2000, "Time series of satellite data: development of new products", NRSP-2 report 99-33, Centre for Geo-Information, Alterra Green World Research, Wageningen.

Schuurmans, J.M., P.A. Troch, A. A. Veldhuizen, W. G. M. Bastiaansen and M. F. P. Bierkens, 2003, "Assimilation of remotely sensed latent heat flux in a distributed hydrological model", Advances in Water Resources 26, 151-159.

Su, Z., 2002, " The surface energy balance system (SEBS) for estimation of turbulent heat fluxes", Hydrol. Earth Sys. Sci. 6(1), 85-99.

Su, Z., A. Yacob, J. Wen, G. Roerink, Y. He, B. Gao, H. Boogaard, C. van Diepen, 2003, "Assessing relative soil moisture with remote sensing data: theory, experimental validation, and application to drought monitoring over the North China Plain", Physics and Chemistry of the Earth 28, 89-101.

Temminghoff, E.J.M., V.J.G. Houba, W. van Vark and G.A. Gaikhorst, 2000. Soil and plant analysis, part 3. Plant analysis procedures. Syllabus Wageningen University, Wageningen, The Netherlands.

Ulaby, F.T., R.K. Moore and A.K. Fung, 1981, "Microwave Remote Sensing, active and passive. Volume 1: microwave remote sensing fundamentals and radiometry".

Van Duivenboden and Cisse, 1989. L' ameriotion de l'alimentation hydrique par des techniques culturales liees à l'interaction eau-fertilisation azotée, Rapport Final.

Verberne, E., G. Dijksterhuis, R. Jongschaap, H. Bazi, A. Sanou and M. Bonzi, 1995. Simulation des cultures pluviales au Burkina Faso (CP-BKF3): sorgho, mil et mais. BuNaSols, InERa, AB-DLO, Ouagadougou, Burkina Faso, Haren, the Netherlands. Series AB-DLO: Note, 18.

Wagner, W, G. Lemoine and H. Rott, 1999 a, "A method for Estimating Soil Moisture from ERS Scatterometer and Soil Data", Remote Sensing of Environment 70, 191-207.

Wagner, W, G. Lemoine and M. Borgeaud, 1999b, "A Study of Vegetation Cover Effects on ERS Scatteromter Data", IEEE Trans. Geoscience and Remote Sensing, Vol. 37, No. 2, 938-948.

Wagner W, and K. Scipal, 2000, "Large-Scale Soil moisture Mapping in Western Africa Using the ERS Scatterometer", IEEE Trans. Geoscience and Remote Sensing, Vol. 38, No. 4, 1777-1782.

Woodhouse, I.H. and D.H. Hoekman, 2000a, "A Model-Based Determination of Soil Moisture Trends in Spain with the ERS–Scatterometer", IEEE Trans. Geoscience and Remote Sensing, Vol. 38, No. 4, 1783 -1793.

Woodhouse, I.H. and D.H. Hoekman, 2000b, "Determining Land Surface Parameters from the ERS-1 Scatterometer" IEEE Trans. Geoscience and Remote Sensing, Vol. 38, No. 1, 126-140.

Appendix 1 NOAA/AVHRR data distribution in year of 2000

Format of Date: month-date-hour-minute

Date: 01-01-08-06	02-02-00-20	03-01-08-24	04-01-00-04
01-02-00-11	02-03-23-35	03-01-23-33	04-05-08-24
01-02-07-55	02-04-08-20	03-02-08-13	04-06-08-12
01-03-23-25	02-05-08-09	03-03-08-12	04-09-00-25
01-06-00-22	02-06-07-57	03-05-00-07	04-10-00-03
01-07-23-36	02-07-00-09	03-09-00-18	04-14-00-13
01-09-08-16	02-08-23-24	03-11-08-10	04-15-08-09
01-11-23-48	02-11-00-20	03-14-23-43	04-15-23-28
01-12-23-25	02-12-23-35	03-18-00-17	04-19-00-01
01-15-00-21	02-13-08-18	03-18-08-30	04-22-08-29
01-16-23-36	02-16-00-08	03-19-23-32	04-23-08-17
01-17-08-25	02-20-00-19	03-23-00-05	04-24-23-26
01-19-08-02	02-21-23-34	03-27-00-16	04-27-00-22
01-20-00-10	02-23-08-04	03-28-23-31	04-28-23-37
01-21-23-25	02-25-00-08	03-29-08-04	
01-24-00-21	02-26-23-22		
01-25-23-36	02-29-23-56		
01-27-08-11			
01-28-08-00			
01-29-00-09			

Date: 05-02-23-48	06-02-00-16	07-01-08-21	08-02-22-01
05-03-23-25	06-03-23-30	07-03-00-20	08-03-08-39
05-06-00-21	06-04-08-33	07-04-20-04	08-04-08-27
05-07-23-36	06-07-00-03	07-04-23-35	08-07-21-46
05-10-08-21	06-11-00-14	07-08-00-08	08-08-21-23
05-11-00-09	06-12-23-28	07-08-08-41	08-11-21-56
05-11-08-10	06-14-08-18	07-09-08-29	08-12-08-34
05-12-23-23	06-16-00-01	07-09-23-32	08-13-08-23
05-15-00-19	06-20-23-49	07-13-23-32	08-16-21-42
05-16-23-34	06-21-08-37	07-16-08-48	08-17-21-18
05-19-08-18	06-21-23-26	07-17-00-05	08-20-08-42
05-20-00-07	06-22-08-25	07-18-23-20	08-21-21-27
05-24-00-17	06-24-00-22	07-21-00-16	08-24-21-59
05-25-23-32	06-25-23-37	07-22-23-30	08-25-21-36
05-26-23-10	06-29-00-10	07-26-00-03	08-26-21-13
05-28-08-14	06-29-08-45	07-26-08-32	08-29-08-37
05-29-00-05	06-30-08-33	07-26-21-19	08-30-08-25
		07-27-08-20	
		07-29-21-52	
		07-30-21-29	

Date: 09-02-21-54	10-03-21-46	11-03-21-38	12-03-21-50
09-03-21-31	10-04-21-23	11-04-21-15	12-04-21-27
09-04-21-08	10-07-21-55	11-07-21-46	12-05-21-04
09-06-22-03	10-08-21-32	11-08-21-23	12-07-21-58
09-07-08-32	10-09-21-09	11-11-21-55	12-08-21-35
09-08-21-17	10-10-08-48	11-12-21-32	12-12-21-43
09-11-21-49	10-11-08-36	11-13-21-09	12-13-21-20
09-12-21-26	10-12-21-41	11-16-21-40	12-16-21-51
09-15-08-39	10-13-21-18	11-17-21-17	12-17-21-28
09-16-08-27	10-16-21-50	11-20-21-48	12-18-21-05
09-17-21-11	10-19-08-43	11-21-21-25	12-22-21-13
09-20-21-43	10-20-21-58	11-22-21-02	12-25-21-44
09-21-21-20	10-21-21-58	11-24-21-56	12-26-21-21
09-24-08-34	10-22-21-12	11-25-21-38	12-30-21-29
09-25-21-29	10-25-21-44	11-26-21-10	12-31-21-06
09-26-21-06	10-26-21-21	11-29-21-42	
09-28-22-01		11-30-21-18	
09-29-21-38			
09-30-21-15			

Appendix 2 Program lists and directory structure

1. For MODIS

The data directory structure for calculation is organized as:
\MODIS
\MODIS\0412
\MODIS\0412\MOD03
\MODIS\0412\MOD09
\MODIS\0412\MOD11
\MODIS\0412\temp (middle way results)
\MODIS\0412\results (final results)
……..

The calculation control file (like 2001control.txt) is located in \MODIS\

In MODIS\HDF-CONVERTER directory

1) Georegister.exe (in \GeoRegister\Debug)
2) HegTools (hegWIN_HDF2GeoTiff.zip)
3) HEG_BatchMode.pro (first read an ascii file to control the calculation dates)
4) LonLat.pro
5) Eos_mosaicking_cutting.pro

The data directory structure for HDF-CONVERTER is organized as:
\MODIS
\MODIS\0412
\MODIS\0412\MOD03
\MODIS\0412\MOD09
\MODIS\0412\MOD11
……..

The calculation control file (like 2001control.txt) is located in \MODIS\

in MODIS\SEBS-MODIS directory

locates the sebs-modis project, including:
1) Albedo_NDVI.pro
2) Process_meteo.pro
3) Ceate_file.pro
4) Evaporation_fract.pro
5) Global_radi.pro
6) Proc_init.pro
7) Surface_ems.pro
8) SEBS_batch_modis.pro

The project also starts with reading an ascii file(like 2001control.txt) to locates the calculation procedures. The data directory structure for SEBS-MODIS is organized as:

\MODIS
\MODIS\0412
\MODIS\0412\temp (middle way results)
\MODIS\0412\MOD09 (final calculation results)
…….

The calculation control file (like 2001control.txt) is located in \MODIS\

2. For HUABEI Evaporation Fraction

The data directory structure is
\Huabei-EF\
\Huabei-EF\HANTS
\Huabei-EF\data
\Huabei-EF\data\results
\Huabei-EF\data\temp

The SEBS-NOAA program files are located in \Huabei-EF
the data as well as the control file for calculation are located in \Huabei-EF\data.
The intermediate results are located in \Huabei-EF\data\temp and the final results are located in \Huabei-EF\data\results

The Evapotranspiration Fraction simulation results are stored in \Huabei-EF\HANTS directory.

3. For SWC data

1) converall.aml (must have the ARC/INFO environment to run)
2) Stacking.pro

the directory structure is organized as
\Peter_van_Oevelen\SWI_decade_China\
\Peter_van_Oevelen\SWI_Month_China\

The program, the data as well as the results are in the same directory.

Appendix 3 SEBS-MODIS IDL project modules

The current SEBS-MODIS IDL project includes the following modules:

1) sebs_batch_modis.pro
This module, named same as the IDL project name, is the start point for the whole program running. It controls the calculations by reading the information from a previous prepared ASCII file under the main calculation folder.

2) proc_init.pro
This module prepares some settings for the calculation, including the paths, input file and output file names as well as the sequences for others modules' calling.

3) global_radi.pro
This module, which calls create_file module to write calculation results, is used to calculate the global radiation.

4) Albedo_NDVI.pro
This module is new created to calculate the albedo and NDVI by using the two bands reflectance. The module also calls the create_file module to write calculation results.

5) surface_ems.pro
This module is used to calculate the emissivity and the result is also written by calling create_file module.

6) process_mete.pro
This module is used to process the ground meteorological data. The calculations results are written into disk-files by using create_file module too.

7) evaporation_fract.pro
This module is used to calculate the evapotranspiration fraction and other components of surface heat fluxes.

8) create_file.pro
The module is developed for the purposes of writing disk data files. The old one, create_file_farr.pro, has been removed from the project since it can not provide map-projection information while writing the data.
Actually, the function of this module can be replaced by using the ENVI internal function ENVI_WRITE_ENVI_FILE.

MODIS data processing
Before using MODIS data and its products, the MODIS data products have to be converted into the ENVI data format, which is the data format used by SEBS.

As referred before, the MODIS data products are published in the format of HDF-EOS. In order to convert EOS-HDF format into ENVI format, a MODIS tool named HEGtools can be used. HEGtools can be used in GUI or command model. For batch processing the MODIS data products, an IDL program has been developed to prepare the parameters for HEGtools and call HEGtools in command mode.

Since there is a problem to extract longitude and latitude information from MOD[03] for SEBS by using HEGtools, another windows executable VC program combined with a IDL program has been developed to obtain the longitude and latitude information for SEBS.

The method for data conversion can be divided into two catalogs: for reflectance and temperature information, first use HEGtools to convert EOS-HDF into GeoTIFF format and then call IDL/ENVI functions to convert it into ENVI format; for geolocation information, first use IDL functions to extract longitude and latitude information form EOS-HDF files and then call Georegister.exe to register longitude/latitude datasets into real world locations in geographic projection and write the results into ENVI format at same time.

The last step for the data preparing is to resize the datasets into same space resolution (1 km) and cut the images into the same calculation areas.

The programs used for MODIS data processing are listed below:

1) HEGtools
These tools can be downloaded from DAAC (http://daac.gsfc.nasa.gov/) and used to convert the HDF-EOS MODIS data files into GeoTIFF format (reflectance and temperature)

2) HEG_BatchMode.pro
This module is developed for converting data in batch model.
It prepares parameters for calling HEGtools and calls HEGtools for Sunzenith, reflectance and temperature datasets to convert the data in GeoTIFF format, and then use the functions from IDL/ENVI to convert GeoTIFF into ENVI format. For the longitude and latitude datasets, it calls LonLat.rpo to extract and register the longitude/latitude datasets into geographic map-projection in ENVI format.
After have the data in the ENVI format, the module also calls eos_mosaick_cutting.pro to generate the needed datasets within the calculation areas.

3) LonLat_Proc.pro
The module is developed to extract longitude/latitude datasets from EOS-HDF files and convert it into ENVI format.

4) eos_mosaick_cutting.pro
This module is developed to generate the exact resolution and extension for the calculations

5) GeoRegister.exe
This module is developed to projection the Longitude/Latitude datasets (or other datasets) extracted from EOS-HDF files by using correspond longitude and latitude information.
Since this module is developed under VC++ environment and it needs another two dynamic link libraries (MSVCP60D.DLL, MFC42D.DLL) to support in the conditions of without VC++ environment installed.

Appendix 4 Boundary conditions

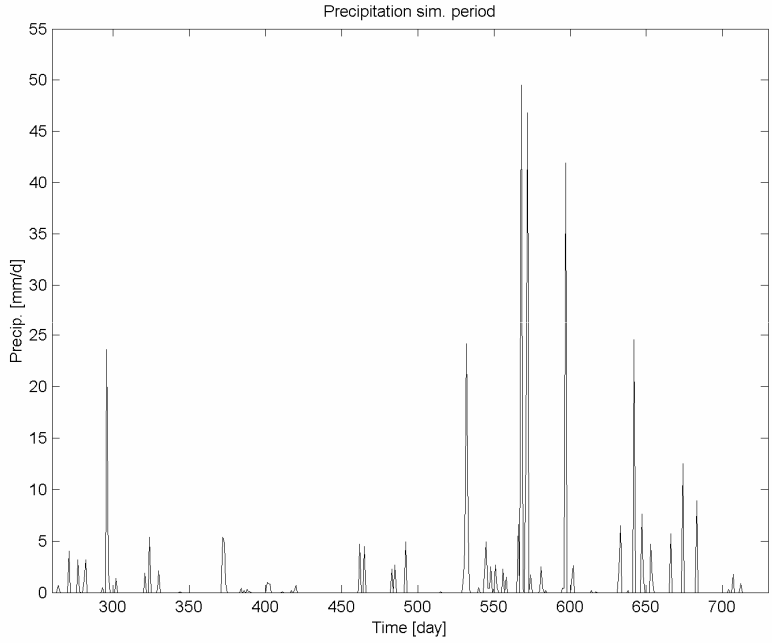

Figure A.1: Precipitation at the meteo-station in the area for the whole simulation period (day 260 in 2000 to the end of 2001).

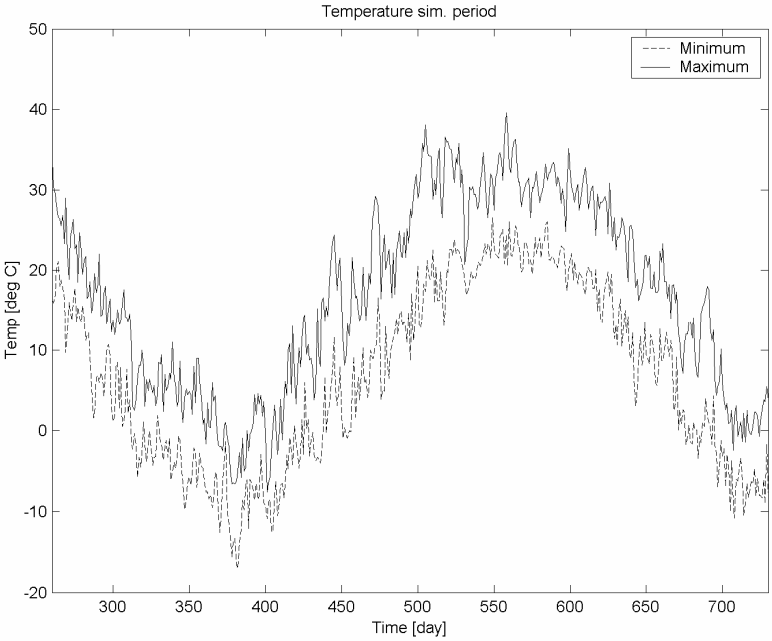

Figure A.2: minimum and maximum temperature at the meteo-station in the area for the whole simulation period (day 260 in 2000 to the end of 2001).

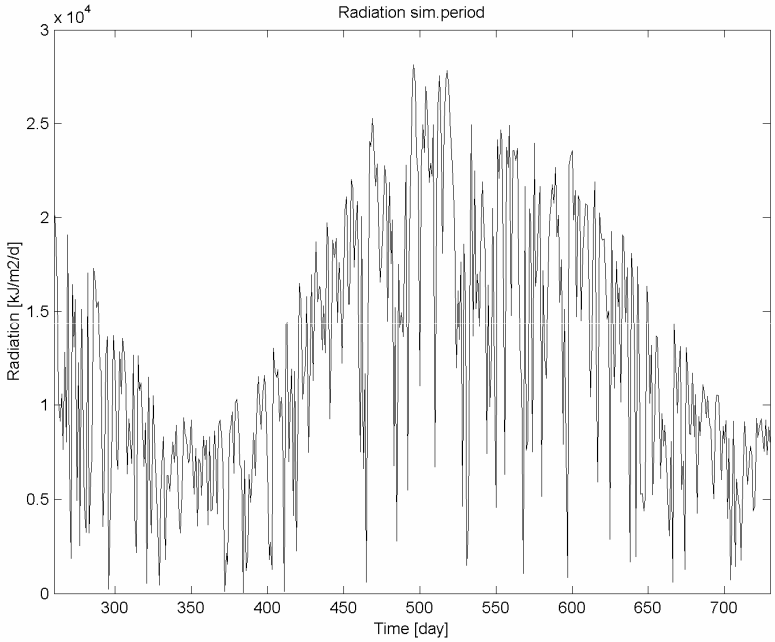

Figure A.3: Irradiation at the meteo-station between 1-1-2000 and 31-12-2000.

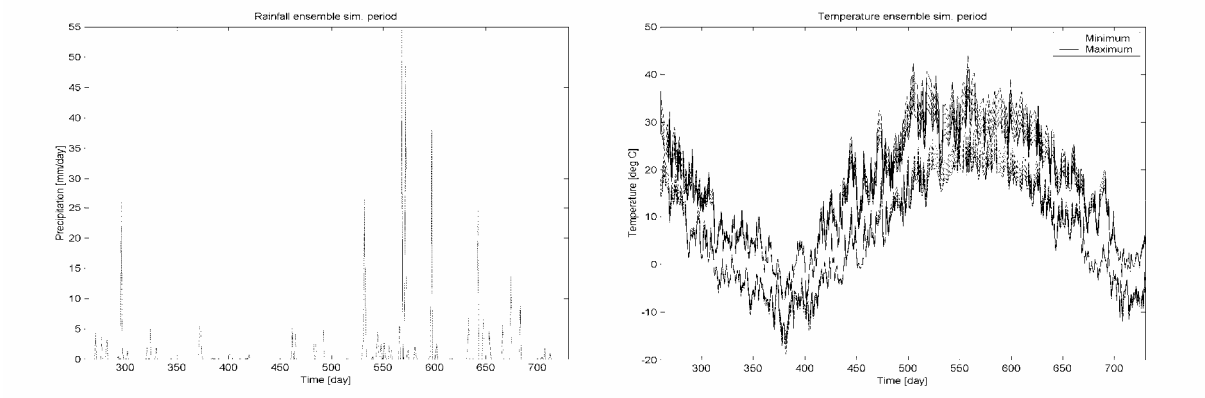

Figure A.4: Meteorological ensembles that were used in the Kalman filter: precipitation (left) and temperature (right). For precipitation the range is +20 % and -20 % of the original value, for temperature -10 % and +10 %.

Appendix 5 Results for all fields

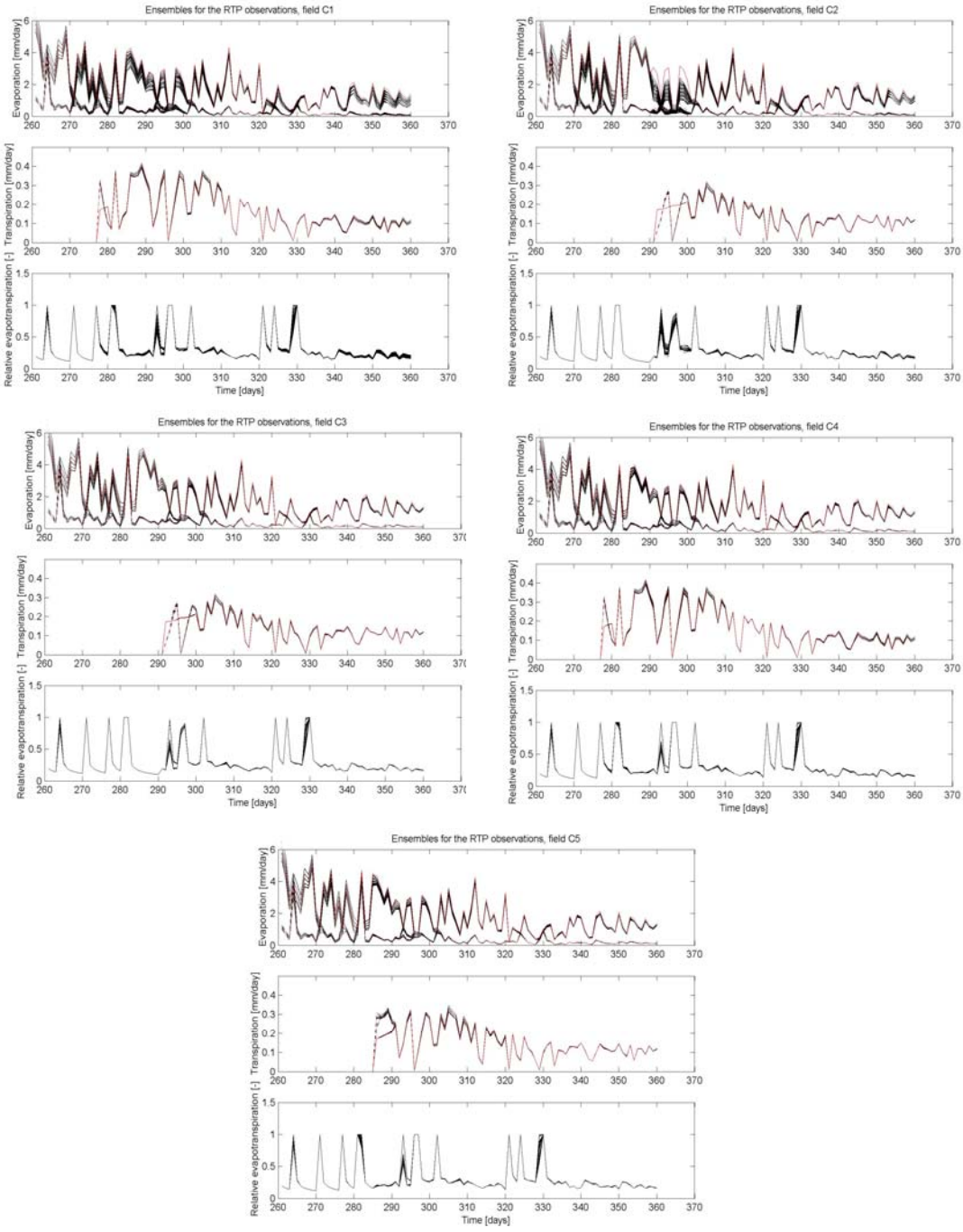

Figure B.1: All modeled fluxes with and without Kalman filtering for fields C1 to C5, for RET observations. Every upper plot is evaporation (potential and actual), middle plots contain potential and actual transpiration and lower plots contain relative evapotranspiration. Black lines represent all ensemble members, the red line is the control run.

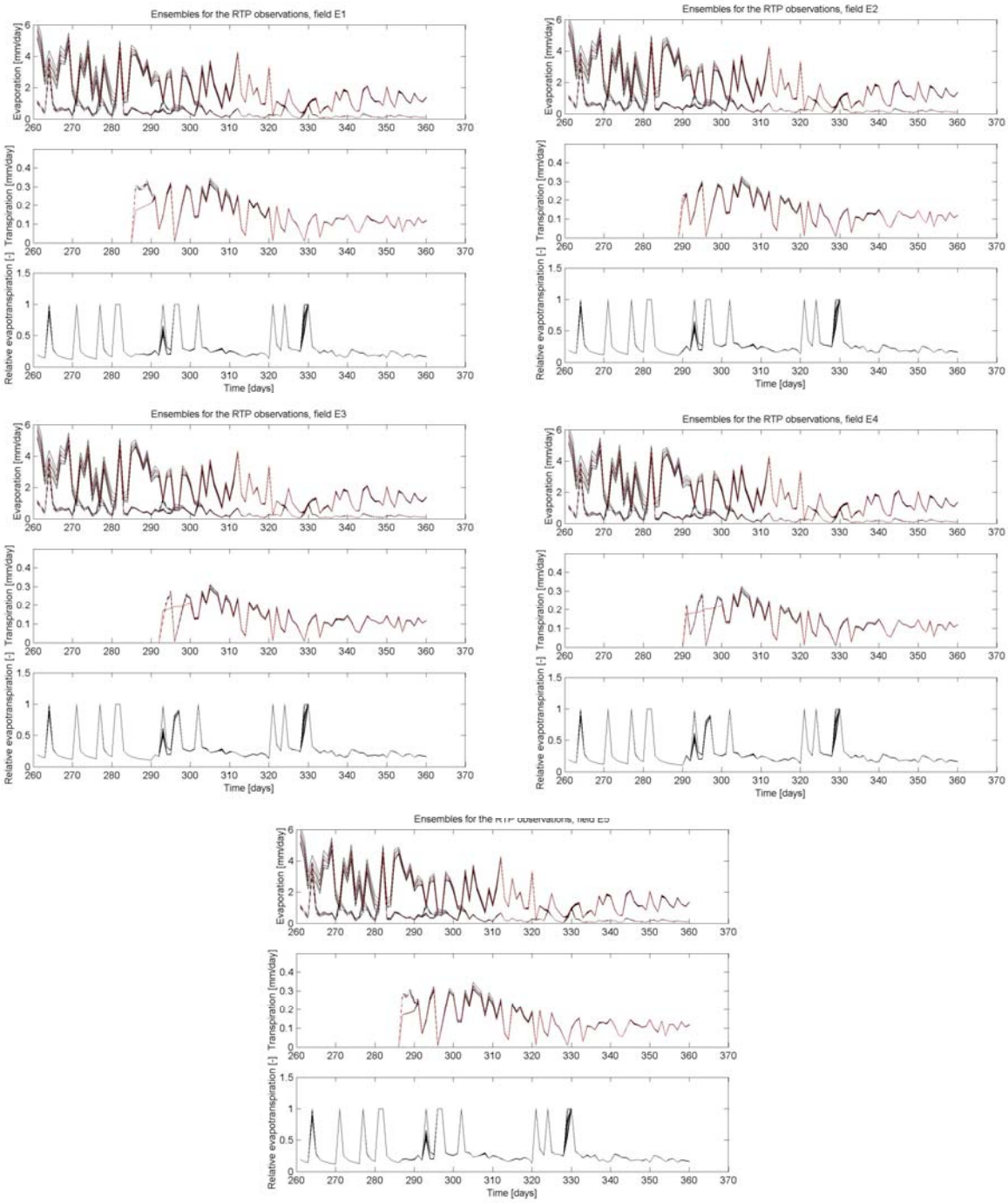

Figure B.2: All modeled fluxes with and without Kalman filtering for fields E1 to E5, for RET observations. Every upper plot is evaporation (potential and actual), middle plots contain potential and actual transpiration and lower plots contain relative evapotranspiration. Black lines represent all ensemble members, the red line is the control run.

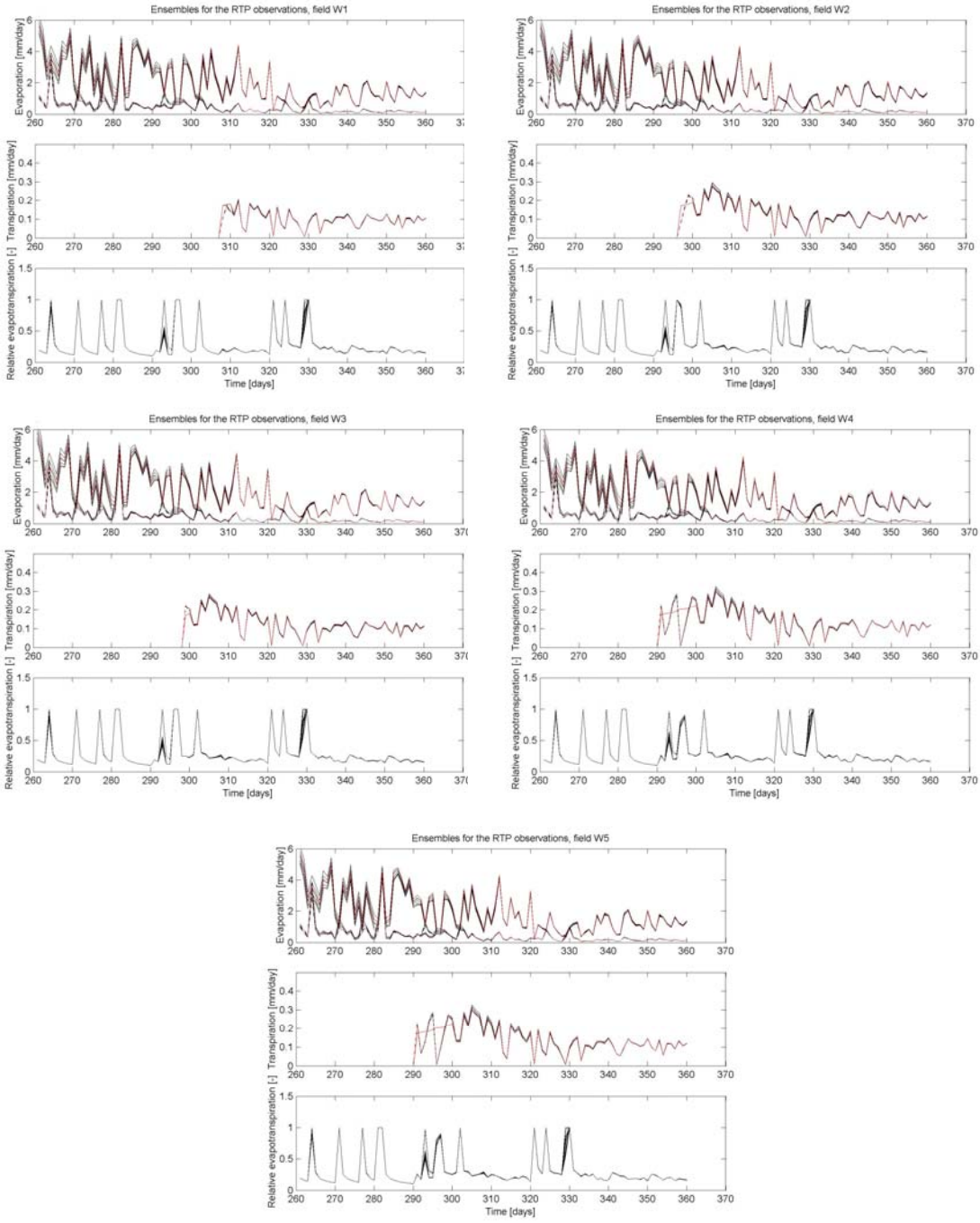

Figure B.3: All modeled fluxes with and without Kalman filtering for fields W1 to W5, for RET observations. Every upper plot is evaporation (potential and actual), middle plots contain potential and actual transpiration and lower plots contain relative evapotranspiration. Black lines represent all ensemble members, the red line is the control run.

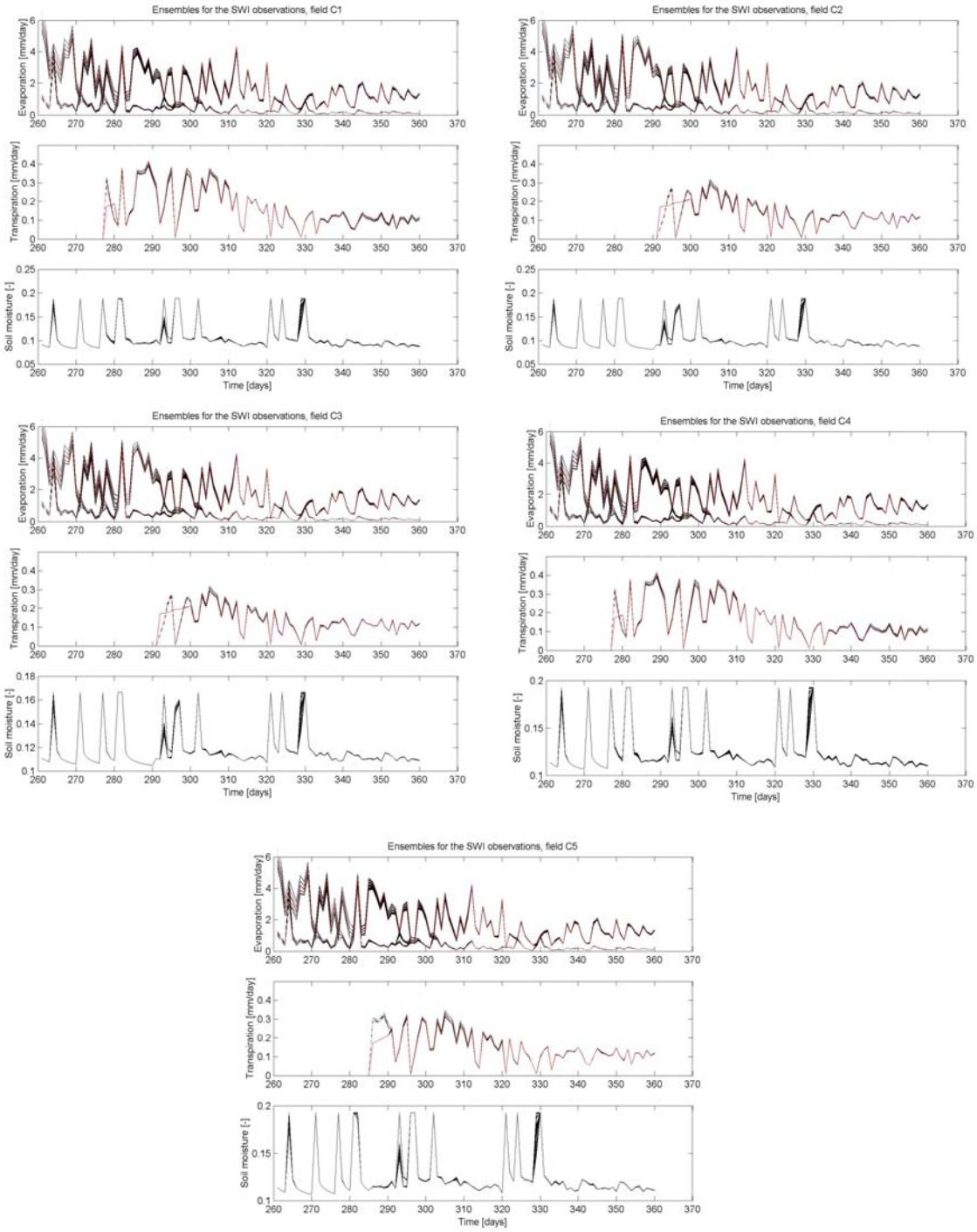

Figure B.4: All modeled fluxes with and without Kalman filtering for fields C1 to C5, for SWI observations. Every upper plot is evaporation (potential and actual), middle plots contain potential and actual transpiration and lower plots contain relative evapotranspiration. Black lines represent all ensemble members, the red line is the control run.

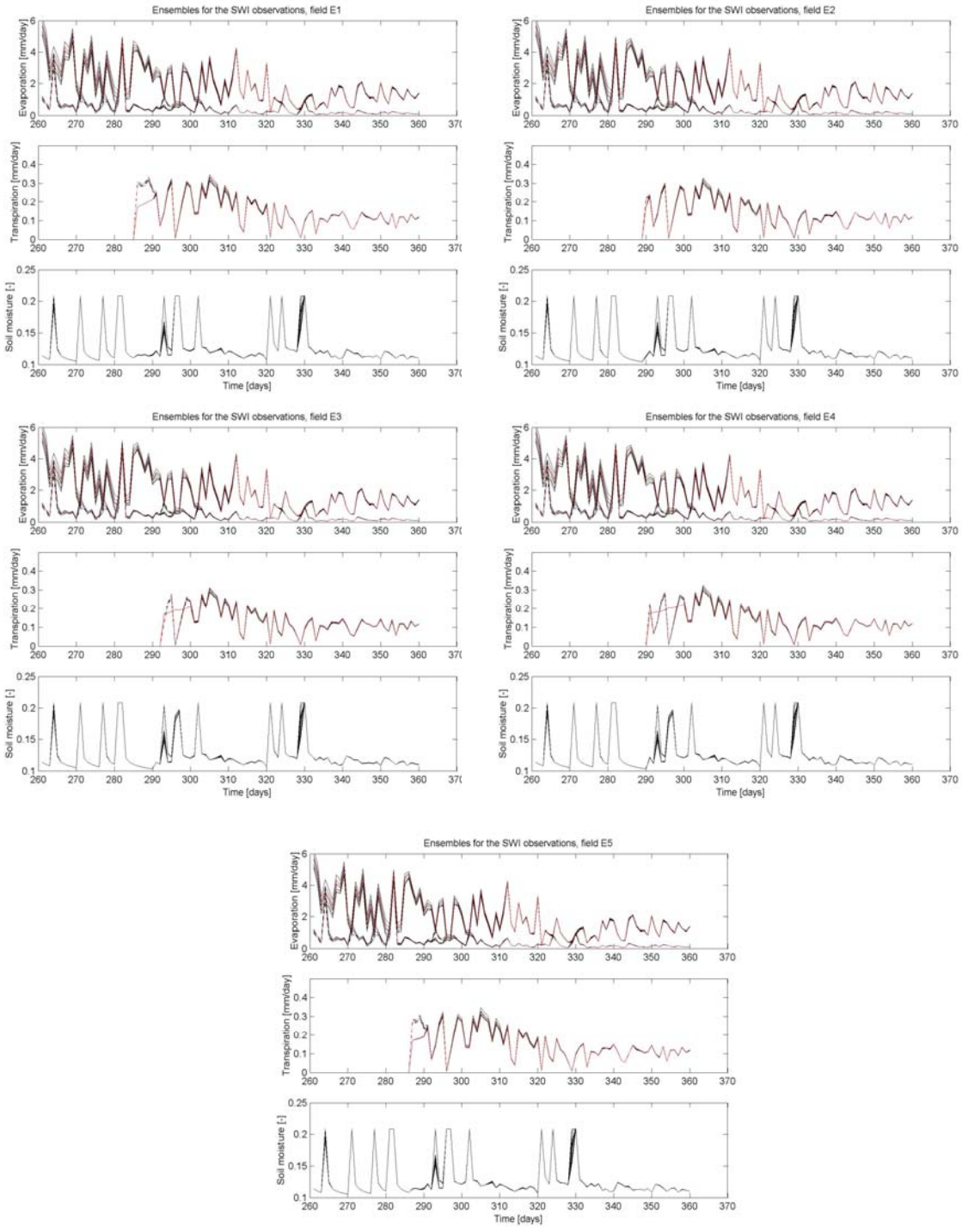

Figure B.5: All modeled fluxes with and without Kalman filtering for fields E1 to E5, for SWI observations. Every upper plot is evaporation (potential and actual), middle plots contain potential and actual transpiration and lower plots contain relative evapotranspiration. Black lines represent all ensemble members, the red line is the control run.

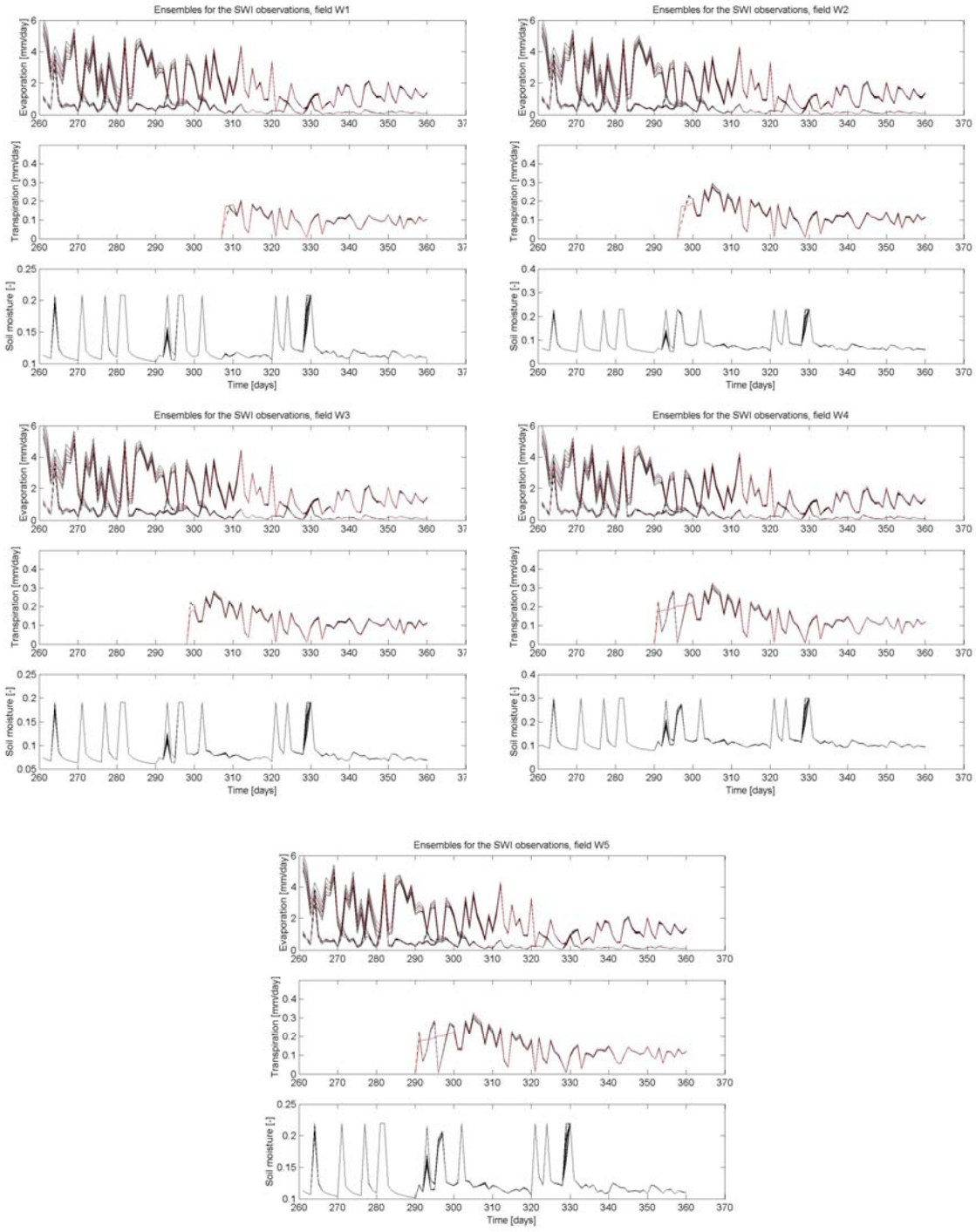

Figure B.6: All modeled fluxes with and without Kalman filtering for fields W1 to W5, for SWI observations. Every upper plot is evaporation (potential and actual), middle plots contain potential and actual transpiration and lower plots contain relative evapotranspiration. Black lines represent all ensemble members, the red line is the control run.

Table B.1: Root mean square errors for all fields, for RETP and SWI observations and with and without updating with the Kalman filter.

Field	RETP – no updating	RETP – with updating	SWI – no updating	SWI – with updating
C1	0.240492	0.241473	0.034879	0.034987
C2	0.240539	0.242095	0.034882	0.034947
C3	0.243566	0.242887	0.019800	0.019822
C4	0.244839	0.244880	0.027751	0.027804
C5	0.231892	0.231080	0.027691	0.027727
E1	0.236762	0.236180	0.033582	0.033612
E2	0.239412	0.238800	0.033551	0.033575
E3	0.251239	0.250626	0.033706	0.033762
E4	0.242392	0.241847	0.033738	0.033762
E5	0.231050	0.230517	0.033571	0.033601
W1	0.303317	0.302388	0.033567	0.033582
W2	0.244075	0.242841	0.062015	0.062130
W3	0.244309	0.244452	0.043078	0.043071
W4	0.242608	0.241030	0.074101	0.074201
W5	0.296231	0.295066	0.038093	0.038140

Appendix 6 Field data Millet experiments

Millet trials with A, B and C type farmers, no fertilizer

Location	Cinzana																			
Farm type:			A					B					C				
Farmer:			Moussa Banaga Diarra					Ousmane Traore					Bakory Fing Traore				
Crop type:	Millet																
Fertilizer:	No																
Harvest number:			1	2	3	4	5	1	2	3	4	5	1	2	3	4	5
Harvest date (Julian day):			197	217	237	259		197	217	237	259		197	217	237	259	
Harvest date:			16-jul-02	05-aug-02	25-aug-02	16-sep-02		16-jul-02	05-aug-02	25-aug-02	16-sep-02		16-jul-02	05-aug-02	25-aug-02	16-sep-02	
Row distance		cm	70	70	70	70	70	80	80	80	80	80	80	80	80	80	
Average number of plants		# 10 m-1	91.0	43.3	20.7	23.3		96.7	35.0	33.7	25.7		41.3	20.7	15.0	17.7	
Plant density		pl ha-1	130000	61905	29524	33333	0	120833	43750	42083	32083	0	51667	25833	18750	22083	
Leaf Area Index		m2 m-2														0.7	
Number of harvested plants			20	20	20	5	5	20	20	20	5	5	20	20	20	5	5
Fresh weight	combs	g									100.00						
	grains	g															
	leaves	g	17.96	47.47				11.00	150.73		100.00		19.80	3.14	100.00		
	stems	g	9.76	20.80				5.25	70.53		650.00		11.91	1.56	75.00		
	roots	g	3.30	8.53				2.00	12.24				0.76	1.18			
Total fresh weight		g	31.02	76.80	0.00	0.00	0.00	18.25	233.50	0.00	850.00	0.00	32.47	117.60	175.00	0.00	0.00
Total fresh weight		kg ha-1	202	238	0	0	0	110	511	0	5454	0	84	152	164	0	0
Sample fresh weight	combs	g				125.00					50.00					100.00	
	grains	g															
	leaves	g	17.96	1.78	200.00	150.00		11.00	52.20	200.00	50.00		19.80	3.14	100.00	100.00	
	stems	g	9.76	0.78	200.00	600.00		5.25	24.43	200.00	300.00		11.91	1.56	75.00	650.00	
	roots	g	3.30	0.32				2.00	4.24				0.76	1.18			
Total sample fresh weight		g	31.02	2.88	400.00	875.00	0.00	18.25	80.87	400.00	400.00	0.00	32.47	5.88	175.00	850.00	0.00
Sample dry weight	combs	g				20.80					8.54					50.37	
	grains	g									0.00						
	leaves	g	2.69	0.14	26.22	40.00		2.35	6.53	39.28	9.25		15.49	0.24	27.77	30.00	
	stems	g	1.90	0.08	23.85	200.00		1.15	3.05	20.67	25.16		3.44	0.14	22.20	300.00	
	roots	g	0.46	0.08				0.06	0.53		0.00		0.04	0.14			
Total sample dry weight		g															
Water content	combs	g g-1				0.83					0.83					0.50	
	grains	g g-1															
	leaves	g g-1	0.85	0.92	0.87	0.73		0.79	0.87	0.80	0.82		0.22	0.92	0.72	0.70	
	stems	g g-1	0.81	0.90	0.88	0.67		0.78	0.87	0.90	0.92		0.71	0.91	0.70	0.54	
	roots	g g-1	0.86	0.75				0.97	0.87				0.95	0.88			
Total water content		g g-1	1.00	1.00	1.00	1.00		1.00	1.00	1.00	1.00		1.00	1.00	1.00	1.00	
Dry weights	combs	kg ha-1	0.0	0.0	0.0	0.0	0.0	0.0	0.0	0.0	109.6	0.0	0.0	0.0	0.0	0.0	0.0
	grains	kg ha-1	0.0	0.0	0.0	0.0	0.0	0.0	0.0	0.0	0.0	0.0	0.0	0.0	0.0	0.0	0.0
	leaves	kg ha-1	17.5	11.6	0.0	0.0	0.0	14.2	41.2	0.0	118.7	0.0	40.0	0.3	26.0	0.0	0.0
	stems	kg ha-1	12.4	6.6	0.0	0.0	0.0	6.9	19.3	0.0	349.8	0.0	8.9	0.2	20.8	0.0	0.0
	roots	kg ha-1	3.0	6.6	0.0	0.0	0.0	0.4	3.3	0.0	0.0	0.0	0.1	0.2	0.0	0.0	0.0
Total dry weight		kg ha-1	32.8	24.8	0.0	0.0	0.0	21.5	63.9	0.0	578.1	0.0	49.0	0.0	46.8	0.0	0.0

Millet trials with A, B and C type farmers, 100 kg ha^{-1} complex fertilizer (17-17-17)

Location	Cinzana																
Farm type:			A					B					C				
Farmer:			Moussa Banaga Diarra					Ousmane Traore					Bakory Fing Traore				
Crop type:	Millet																
Fertilizer:	Yes																
Harvest number:			1	2	3	4	5	1	2	3	4	5	1	2	3	4	5
Harvest date (Julian day):			197	217	237	259		197	217	237	259		197	217	237	259	
Harvest date:			16-jul-02	05-aug-02	25-aug-02	16-sep-02		16-jul-02	05-aug-02	25-aug-02	16-sep-02		16-jul-02	05-aug-02	25-aug-02	16-sep-02	
Row distance		cm	80	80	80	80	80	80	80	80	80	80	80	80	80	80	
Average number of plants		# 10 m-1		40.0	29.7	31.0			41.7	41.3	30.0		46.7	23.3	20.3	24.7	
Plant density		pl ha-1	0	50000	37083	38750	0	0	52083	51667	37500	0	58333	29167	25417	30833	
Leaf Area Index		m2 m-2															
Number of harvested plants				20	20	5		20	20	20	5		20	20	20	5	
Fresh weight	combs	g		0.00													
	grains	g		0.00													
	leaves	g		749.85					443.33					261.38			
	stems	g		743.62					201.06					131.42			
	roots	g		106.54					55.61					40.38			
Total fresh weight		g	0.00	1600.01	0.00	0.00	0.00	0.00	700.00	0.00	0.00	0.00	35.31	433.18	0.00	0.00	0.00
Total fresh weight		kg ha-1	#DIV/0!	4000	0	0	#DIV/0!	0	1823	0	0	#DIV/0!	103	632	0	0	#DIV/0!
Sample fresh weight	combs	g		0.00		200.00					150.00					200.00	
	grains	g		0.00													
	leaves	g		191.54	500.00	250.00			100.52	500.00	200.00			3.56	250.00	200.00	
	stems	g		189.95	550.00	1000.00			45.59	750.00	900.00			1.79	200.00	1250.00	
	roots	g		27.21					12.61					0.55			
Total sample fresh weight		g	0.00	408.70	1050.00	1450.00		0.00	158.72	1250.00	1250.00	0.00	0.00	5.90	450.00	1650.00	0.00
Sample dry weight	combs	g		0.00		58.30					60.00					83.33	
	grains	g		0.00													
	leaves	g		24.66	65.09	50.00			8.99	82.76	25.00			0.67	42.79	100.00	
	stems	g		15.28	112.83	45.00			5.73	201.72	250.00			0.35	18.46	500.00	
	roots	g		10.93					2.65					0.18			
Total sample dry weight		g	0.00	50.87	177.92	153.30	0.00	0.00	17.37	284.48	335.00	0.00	5.73	1.20	61.25	683.33	0.00
Water content	combs	g g-1				0.71					0.60					0.58	
	grains	g g-1															
	leaves	g g-1		0.87	0.87	0.80			0.91	0.83	0.88			0.81	0.83	0.50	
	stems	g g-1		0.92	0.79	0.96			0.87	0.73	0.72			0.80	0.91	0.60	
	roots	g g-1		0.60					0.79					0.67			
Total water content		g g-1		0.88	0.83	0.89			0.89	0.77	0.73			0.80	0.86	0.59	
Dry weights	combs	kg ha-1	0.0	0.0	0.0	0.0	0.0	0.0	0.0	0.0	0.0	0.0	0.0	0.0	0.0	0.0	0.0
	grains	kg ha-1	0.0	0.0	0.0	0.0	0.0	0.0	0.0	0.0	0.0	0.0	0.0	0.0	0.0	0.0	0.0
	leaves	kg ha-1	0.0	241.3	0.0	0.0	0.0	0.0	103.3	0.0	0.0	0.0	0.0	71.7	0.0	0.0	0.0
	stems	kg ha-1	0.0	149.6	0.0	0.0	0.0	0.0	65.8	0.0	0.0	0.0	0.0	37.5	0.0	0.0	0.0
	roots	kg ha-1	0.0	106.9	0.0	0.0	0.0	0.0	30.4	0.0	0.0	0.0	0.0	19.3	0.0	0.0	0.0
Total dry weight		kg ha-1	0.0	497.9	0.0	0.0	0.0	0.0	199.5	0.0	0.0	0.0	0.0	0.0	0.0	0.0	0.0

Appendix 7 Field data Sorghum experiments

Sorghum trials, A, B and C type farmers, no fertilizer

Location	Konobougou																			
Farm type:																				
Farmer:				A Nianzon Diarra						B Zoumana Diarra						C Modibo Keita				
Crop type:	Sorghum																			
Fertilizer:	No																			
Harvest number:			1	2	3	4	5		1	2	3	4	5		1	2	3	4	5	
Harvest date (Julian day):			197	217	237	257			197	217	237	257			197	217	237	257		
Harvest date:			16-jul-02	05-aug-02	25-aug-02	14-sep-02			16-jul-02	05-aug-02	25-aug-02	14-sep-02			16-jul-02	05-aug-02	25-aug-02	14-sep-02		
Row distance		cm	70	70	70	70			70	70	70	70			70	70	70	70		
Number of plants		# 10 m-1	81	80	83	80				74	84	82				73	75	74		
Plant density		pl ha-1	115714	113810	118095	113810	#DIV/0!		0	105714	119524	117143	#DIV/0!		0	104762	107619	105714		
Leaf Area Index		m2 m-2								14.56										
Number of harvested plants			20	10	10	5			20	10	10	5			20	10	10	5		
Fresh weight	combs	g				22.00						6.00						50.00		
	grains	g																		
	leaves	g	26.00	82.00	256.00	290.00			22.00	76.00	182.00	143.00			44.00	64.00	162.00	170.00		
	stems	g	3.00	86.00	368.00	902.00			3.00	70.00	270.00	432.00			8.00	58.00	284.00	501.00		
	roots	g	0.60	17.00	62.00	94.00			8.00	14.00	38.00	38.00			6.00	20.00	44.00	41.00		
Total fresh weight		g	29.60	185.00	686.00	1308.00	0.00		33.00	160.00	490.00	619.00	0.00		58.00	142.00	490.00	762.00	0.00	
Total fresh weight		kg ha-1	171	2105	8101	29773	#DIV/0!		0	1691	5857	14502	#DIV/0!		0	1488	5273	16111	#DIV/0!	
Sample fresh weight	combs	g				22.00						6.00						22.00		
	grains	g																		
	leaves	g	26.00	82.00	256.00	290.00			22.00	76.00	182.00	143.00			44.00	64.00	162.00	290.00		
	stems	g	3.00	86.00	368.00	902.00			3.00	70.00	270.00	432.00			8.00	58.00	284.00	902.00		
	roots	g	0.60	17.00	62.00	94.00			8.00	14.00	38.00	38.00			6.00	20.00	44.00	94.00		
Total sample fresh weight		g	29.60	185.00	686.00	1308.00			33.00	160.00	490.00	619.00	0.00		58.00	142.00	490.00	1308.00	0.00	
Sample dry weight	combs	g				6.00						0.00						4.00		
	grains	g																0.00		
	leaves	g	3.24			96.00			3.06			54.00						63.00		
	stems	g	0.09			300.00			0.09			140.00						148.00		
	roots	g	0.06			39.00			0.62			16.00						15.00		
Total sample dry weight		g	3.39	0.00	0.00	441.00	0.00		3.77	0.00	0.00	210.00	0.00		0.00	0.00	0.00	230.00	0.00	
Water content	combs	g g-1				0.73						1.00						0.82		
	grains	g g-1																		
	leaves	g g-1	0.88	1.00	1.00	0.67			0.86	1.00	1.00	0.62			1.00	1.00	1.00	0.78		
	stems	g g-1	0.97	1.00	1.00	0.67			0.97	1.00	1.00	0.68			1.00	1.00	1.00	0.84		
	roots	g g-1	0.90	1.00	1.00	0.59			0.92	1.00	1.00	0.58			1.00	1.00	1.00	0.84		
Total water content		g g-1	0.89	1.00	1.00	0.66			0.89	1.00	1.00	0.66			1.00	1.00	1.00	0.82		
Dry weights	combs	kg ha-1	0.0	0.0	0.0	136.6	0.0		0.0	0.0	0.0	0.0	0.0		0.0	0.0	0.0	192.2	0.0	
	grains	kg ha-1	0.0	0.0	0.0	0.0	0.0		0.0	0.0	0.0	0.0	0.0		0.0	0.0	0.0	0.0	0.0	
	leaves	kg ha-1	18.7	0.0	0.0	2185.1	0.0		0.0	0.0	0.0	1265.1	0.0		0.0	0.0	0.0	780.8	0.0	
	stems	kg ha-1	0.5	0.0	0.0	6828.6	0.0		0.0	0.0	0.0	3280.0	0.0		0.0	0.0	0.0	1738.0	0.0	
	roots	kg ha-1	0.3	0.0	0.0	887.7	0.0		0.0	0.0	0.0	374.9	0.0		0.0	0.0	0.0	138.3	0.0	
Total dry weight		kg ha-1	19.6	0.0	0.0	10038.0	0.0		0.0	0.0	0.0	4920.0	0.0		0.0	0.0	0.0	2849.4	0.0	

Sorghum trials, A, B and C type farmers, 100 kg ha^{-1} complex fertilizer (17-17-17)

Location	Konobougou																			
Farm type:																				
Farmer:				A Nianzon Diarra						B Zoumana Diarra						C Modibo Keita				
Crop type:	Sorghum																			
Fertilizer:	Yes																			
Harvest number:			1	2	3	4	5		1	2	3	4	5		1	2	3	4	5	
Harvest date (Julian day):			197	217	237	257			197	217	237	257			197	217	237	257		
Harvest date:			16-jul-02	05-aug-02	25-aug-02	14-sep-02			16-jul-02	05-aug-02	25-aug-02	14-sep-02			16-jul-02	05-aug-02	25-aug-02	14-sep-02		
Row distance		cm	70	70	70	70			70	70	70	70			70	70	70	70		
Average number of plants		# 10 m-1	78.33	77.33	82.00	79.33				74.33	81.67	78.33				75.33	77.33	76.00		
Plant density		pl ha-1	111905	110476	117143	113333	#DIV/0!		0	106190	116667	111905	#DIV/0!		0	107619	110476	108571		
Leaf Area Index		m2 m-2																		
Number of harvested plants			20	10	10	5			0	10	10	5			20	10	10	5		
Fresh weight	combs	g				46.00						34.00						30.00		
	grains	g																		
	leaves	g		260.00	514.00	344.00				236.00	412.00	248.00				162.00	394.00	312.00		
	stems	g		284.00	1390.00	1420.00				332.00	1070.00	802.00				218.00	932.00	1085.00		
	roots	g		44.00	184.00	142.00				42.00	93.00	114.00				42.00	108.00	30.00		
Total fresh weight		g	0.00	588.00	2088.00	1952.00	0.00		0.00	610.00	1575.00	1198.00	0.00		0.00	422.00	1434.00	1457.00	0.00	
Total fresh weight		kg ha-1	0	6496	24459	44245	#DIV/0!		#DIV/0!	6478	18375	26812	#DIV/0!		0	4542	15842	31638	#DIV/0!	
Sample fresh weight	combs	g				46.00						34.00						30.00		
	grains	g																		
	leaves	g		260.00	514.00	344.00				236.00	412.00	248.00				162.00	394.00	312.00		
	stems	g		284.00	1390.00	1420.00				332.00	1070.00	802.00				218.00	932.00	1085.00		
	roots	g		44.00	184.00	142.00				42.00	93.00	114.00				42.00	108.00	30.00		
Total sample fresh weight		g	0.00	588.00	2088.00	1952.00			0.00	610.00	1575.00	1198.00	0.00		0.00	422.00	1434.00	1457.00	0.00	
Sample dry weight	combs	g				8.00						3.00						6.00		
	grains	g										0.00								
	leaves	g				130.00						80.00						122.00		
	stems	g				614.00						248.00						400.00		
	roots	g				56.00						41.00						52.00		
Total sample dry weight		g	0.00	0.00	0.00	808.00	0.00		0.00	0.00	0.00	372.00	0.00		0.00	0.00	0.00	580.00	0.00	
Water content	combs	g g-1				0.83						0.91						0.80		
	grains	g g-1																		
	leaves	g g-1		1.00	1.00	0.62				1.00	1.00	0.68				1.00	1.00	0.61		
	stems	g g-1		1.00	1.00	0.57				1.00	1.00	0.69				1.00	1.00	0.63		
	roots	g g-1		1.00	1.00	0.61				1.00	1.00	0.64				1.00	1.00	-0.73		
Total water content		g g-1		1.00	1.00	0.59				1.00	1.00	0.69				1.00	1.00	0.60		
Dry weights	combs	kg ha-1	0.0	0.0	0.0	181.3	0.0		0.0	0.0	0.0	67.1	0.0		0.0	0.0	0.0	130.3	0.0	
	grains	kg ha-1	0.0	0.0	0.0	0.0	0.0		0.0	0.0	0.0	0.0	0.0		0.0	0.0	0.0	0.0	0.0	
	leaves	kg ha-1	0.0	0.0	0.0	2946.7	0.0		0.0	0.0	0.0	1790.5	0.0		0.0	0.0	0.0	2649.1	0.0	
	stems	kg ha-1	0.0	0.0	0.0	13917.3	0.0		0.0	0.0	0.0	5550.5	0.0		0.0	0.0	0.0	8685.7	0.0	
	roots	kg ha-1	0.0	0.0	0.0	1269.3	0.0		0.0	0.0	0.0	917.6	0.0		0.0	0.0	0.0	1129.1	0.0	
Total dry weight		kg ha-1	0.0	0.0	0.0	18314.7	0.0		0.0	0.0	0.0	8325.7	0.0		0.0	0.0	0.0	12594.3	0.0	